



## Reconciling the bottom-up and top-down estimates of the methane chemical sink using multiple observations

Yuanhong Zhao<sup>1,2</sup>, Marielle Saunois<sup>2</sup>, Philippe Bousquet<sup>2</sup>, Xin Lin<sup>2</sup>, Michaela I. Hegglin<sup>3, 4</sup>, Josep G. Canadell<sup>5</sup>, Robert B. Jackson<sup>6</sup>, and Bo Zheng<sup>7</sup>

5

<sup>1</sup>College of Oceanic and Atmospheric Sciences, Ocean University of China, Qingdao, 266100, People's Republic of China

<sup>2</sup>Laboratoire des Sciences du Climat et de l'Environnement, LSCE-IPSL (CEA-CNRS-UVSQ), Université Paris-Saclay, 91191 Gif-sur-Yvette, France

10 <sup>3</sup> Institute of Energy and Climate Research – Stratosphere (IEK-7), Forschungszentrum Jülich GmbH, 52425 Jülich, Germany.

<sup>4</sup> Department of Meteorology, University of Reading, Earley Gate, Reading RG6 6BB, United Kingdom

<sup>5</sup> Global Carbon Project, CSIRO Oceans and Atmosphere, Canberra, Australian Capital Territory 2601, Australia

15 <sup>6</sup> Earth System Science Department, Woods Institute for the Environment, and Precourt Institute for Energy, Stanford University, Stanford, CA 94305, USA

<sup>7</sup> Institute of Environment and Ecology, Tsinghua Shenzhen International Graduate School, Tsinghua University, Shenzhen 518055, China.

20 *Correspondence to:* Yuanhong Zhao (zhaoyuanhong@ouc.edu.cn)

25

30



35 **Abstract**

The methane chemical sink estimated by atmospheric chemistry models (bottom-up method) is significantly larger than estimates based on methyl-chloroform (MCF) inversions (top-down method). The difference is partly attributable to large uncertainties in hydroxyl radical (OH) concentrations simulated by the atmospheric chemistry models used to derive the bottom-up estimates. In this study, we propose a new approach based on OH precursor observations and a chemical box model. This approach improves the 3-dimensional distributions of tropospheric OH radicals obtained from atmospheric chemistry models and reconciles the bottom-up and top-down estimates of the methane sink due to chemical loss. By constraining the model simulated OH precursors with observations, the global tropospheric mean OH concentration ( $[\text{OH}]_{\text{trop-M}}$ ) is  $\sim 10 \times 10^5 \text{ molec cm}^{-3}$  (which is  $2 \times 10^5 \text{ molec cm}^{-3}$  lower than the original model-simulated global  $[\text{OH}]_{\text{trop-M}}$ ) and agrees with that obtained by the top-down method based on MCF inversions. With the OH constrained by precursor observations, the methane chemical loss is 471-508  $\text{Tg yr}^{-1}$  averaged from 2000 to 2009. The new adjusted estimate is more consistent with the top-down estimates in the recent global methane budget by the Global Carbon Project (GCP) (459-516  $\text{Tg yr}^{-1}$ ) than the bottom-up estimates using the original model-simulated OH fields (577-612  $\text{Tg yr}^{-1}$ ). The overestimation of global  $[\text{OH}]_{\text{trop-M}}$  and methane chemical loss simulated by the atmospheric chemistry models is caused primarily by the models' underestimation of carbon monoxide and total ozone column, and overestimation of nitrogen dioxide. Our results highlight that constraining the model simulated OH fields with available OH precursor observations can help improve the bottom-up estimated methane sink.

55

60



## Introduction

Methane ( $\text{CH}_4$ ) is a potent greenhouse gas, with its 100-year global warming potential 27 (for non-fossil  $\text{CH}_4$ ) and 30 times (for fossil  $\text{CH}_4$ ) times that of  $\text{CO}_2$  (Forster et al., 2021). The tropospheric  $\text{CH}_4$  mixing ratios have increased by more than 1.6 times between pre-industrial and the present day, 65 resulting in  $0.54 \pm 0.11 \text{ W m}^{-2}$  radiative forcing from 1750 to 2019 (Forster et al., 2021). After a short-term stabilization during 2000-2006, the atmospheric methane mixing ratio rose increasingly quickly from  $5 \text{ ppbv yr}^{-1}$  in 2006 to  $17 \text{ ppbv yr}^{-1}$  in 2021 based on surface networks (Dlugokencky, NOAA/GML, 2022). The rapid growth in atmospheric  $\text{CH}_4$  over the recent decade further challenges meeting the  $1.5\text{-}2.0^\circ\text{C}$  targets of the Paris Agreement (Nisbet et al., 2019) and therefore is becoming an 70 increasing concern (Jackson et al. 2020).

Understanding the drivers of atmospheric methane changes rely on accurate estimates of the global methane budget, as methane concentrations in the atmosphere are the net balance between emissions and sinks. To estimate this budget, the Global Carbon Project (GCP) has established the global  $\text{CH}_4$  75 budget by gathering up-to-date observations and model information (Kirschke et al. 2013; Saunio et al., 2016; 2017; 2020). One of the remaining largest uncertainties, as pointed out by the most recent  $\text{CH}_4$  budget (Saunio et al., 2020), is the chemical loss of  $\text{CH}_4$ . The chemical loss of  $\text{CH}_4$  stems mainly through the reaction of  $\text{CH}_4$  with hydroxyl radical ( $\text{OH}$ ), which is also the most important  $\text{CH}_4$  sink.

80 The hydroxyl radical ( $\text{OH}$ ) is a key species in tropospheric chemistry that reacts with most greenhouse gases and air pollutants (Levy, 1971), being the main oxidant of the lower atmosphere. Due to its extremely short lifetime (typically 1 second) and spatial variability, direct observations do not allow for the quantification of the global  $[\text{OH}]$  distributions. The  $[\text{OH}]$  for calculating the chemical sink of  $\text{CH}_4$  is thus estimated either from top-down or bottom-up methods. The top-down method estimates  $[\text{OH}]$



85 mainly through inversions constrained by independent observations of 1-1-1trichloroethane (methyl  
chloroform, MCF), assuming that emissions of this compound are well known. Such MCF-based top-  
down method has been widely used in the scientific community to derive OH trends but it can only  
yield the global to latitudinal mean [OH] due to the sparse MCF observations and does not represent the  
chemical feedback on OH (e.g., Prinn et al., 2001; Bousquet et al., 2005; Montzka et al., 2011; Naus et  
90 al., 2021; Patra et al., 2020). Bottom-up approaches on the other hand simulate the [OH] by atmospheric  
chemistry models to account for the chemical mechanisms that determine OH production and loss, but  
their estimates of the global mean [OH] usually disagree with MCF-based estimates (Naik et al., 2013;  
Zhao et al., 2019).

95 The global [OH] estimated by bottom-up model-based and top-down MCF-based methods are different  
in magnitudes, inter-annual variations, and trends, resulting in large differences in estimated CH<sub>4</sub> sinks  
between the two methods. In the last global CH<sub>4</sub> budget, most of the OH fields used to estimate the  
bottom-up CH<sub>4</sub> sink were obtained from the atmospheric chemistry models that participated in the  
IGAC/SPARC Chemistry-Climate Model Initiative Phase-1 (CCMI-1) project. However, these models  
100 showed a wide range of  $9.4\text{--}14.4 \times 10^5 \text{ molec cm}^{-3}$  in global airmass-weighted tropospheric mean [OH]  
([OH]<sub>trop-M</sub>) (Zhao et al., 2019; Saunois et al., 2020), thus mostly higher than the values estimated by  
the MCF-based inversions ( $\sim 10 \times 10^5 \text{ molec cm}^{-3}$ ; Prinn et al., 2001; Bousquet et al., 2005). Indeed, the  
mean CH<sub>4</sub> chemical loss for 2000-2009, as calculated by bottom-up approaches, is  $595 \text{ Tg yr}^{-1}$  (range  
489-749 Tg yr<sup>-1</sup>), much higher than the  $505 \text{ Tg yr}^{-1}$  (range 459-516 Tg yr<sup>-1</sup>) estimated by top-down CH<sub>4</sub>  
105 inversions (Saunois et al., 2020). Those top-down inversions using box models conclude that decreased  
[OH] and therefore CH<sub>4</sub> chemical loss after the mid-2000s can explain the resumed CH<sub>4</sub> increase since  
2006 (Turner et al., 2017; Rigby et al., 2017) while more recent 3D inversions show no significant trend  
in [OH] after 2000 (Naus et al., 2021; Patra et al., 2021). In contrast to top-down MCF-based inversions,

atmospheric chemistry models simulate a continuous increase in [OH] and consequently CH<sub>4</sub> chemical  
110 loss from the 1980s (Zhao et al., 2020b).

Reconciling the bottom-up and top-down estimates of the methane chemical sink is essential for a more  
accurate estimate of the global methane budget and to better attribute the observed changes in  
atmospheric growth rates of CH<sub>4</sub>. One way to improve the bottom-up estimates of the CH<sub>4</sub> sink and thus  
115 reconcile the difference is to correct the [OH] simulated by atmospheric models using observations of  
OH precursors. Indeed, uncertainties in the [OH] simulated by atmospheric models can be attributed to  
biases in precursor concentrations. For example, Naik et al. (2013) found that an underestimation of  
carbon monoxide (CO) in the Northern Hemisphere can contribute to the overestimation of [OH] in this  
hemisphere; Strode et al. (2015) estimated that removing the model bias in O<sub>3</sub> and water vapor (H<sub>2</sub>O<sub>(g)</sub>)  
120 and reducing northern hemispheric nitrogen oxides (NO<sub>x</sub>=NO+NO<sub>2</sub>) emissions can reduce a high bias in  
the global OH burden by 10%. In addition, the budget analysis of OH production and loss showed that  
about 90% of OH production is directly related to stratospheric and tropospheric ozone (O<sub>3</sub>), H<sub>2</sub>O<sub>(g)</sub>, and  
nitrogen oxide (NO), and ~60% of OH is removed by reaction with CO, CH<sub>4</sub> and formaldehyde (CH<sub>2</sub>O)  
(Lelieveld et al., 2016; Zhao et al., 2020b). Thus, bottom-up estimates of the CH<sub>4</sub> sink from chemistry  
125 transport models can be improved if one can reduce the biases due to these OH precursors in modeled  
[OH].

Fortunately, several satellites have collected long-term continuous observations of the aforementioned  
OH precursors with global coverage, providing the opportunity to evaluate and improve bottom-up  
130 estimates of the CH<sub>4</sub> sink. In this context, the main objective of this study is to reconcile the bottom-up  
and top-down estimates of the CH<sub>4</sub> sink by improving the atmospheric model simulated OH fields using  
multiple satellite observations and meteorological data from reanalysis. As a result, top-down estimates



of CH<sub>4</sub> emissions will also benefit from the improved 3D distributions of [OH] (Zhao et al., 2020a; Saunois et al. 2020). We first evaluate the OH precursors (CO, CH<sub>4</sub>, O<sub>3</sub>, CH<sub>2</sub>O, and NO<sub>2</sub>, the total column O<sub>3</sub>, and H<sub>2</sub>O<sub>(g)</sub>) simulated for the year 2010 by the CESM1-CAM4chem and GEOSCCM; these  
135 models participated in the CCMI-1 project and were used to estimate the global methane sink in Saunois et al. (2020) and represent two different chemical mechanisms. We then estimate the observation-based OH fields by correcting model biases of the two modeled OH fields due to the above-mentioned OH precursors using the Dynamically Simple Model of Atmospheric Chemical Complexity  
140 (DSMACC). By doing so, we quantify the bias in tropospheric [OH] attributable to each precursor. Finally, we estimate the chemical sink of CH<sub>4</sub> using the observation-based OH field and, based on the uncertainties inferred for [OH], we reveal the dominant factors contributing to the uncertainties in CH<sub>4</sub> chemical sink at the global and regional scales.

## 145 2 Method

### 2.1 Observational data

The total column O<sub>3</sub>, which mainly influences the O (<sup>1</sup>D) photolysis rate, is constrained by the National Aeronautics and Space Administration (NASA) Solar Backscatter Ultraviolet (SBUV) Merged Ozone Data Set (MOD) (Frith et al., 2014). The SBUV/MOD column O<sub>3</sub> data are derived by combining  
150 observations from nine SBUV-type instruments aboard the NASA Aura satellite. The monthly 5° zonal mean O<sub>3</sub> columns are available from January 1970 to December 2018.

Tropospheric O<sub>3</sub> is important in determining OH production. We constrain its spatial distributions using the tropospheric column O<sub>3</sub> data from the combined Aura Ozone Monitoring Instrument/Microwave  
155 Limb Sounder (OMI/MLS) satellite observations, which are generated by subtracting the co-located MLS limb measurements (integrated over the stratosphere to derive stratospheric column ozone) from

total column ozone retrieved by OMI, an Ultraviolet/Visible nadir solar backscatter spectrometer (Ziemke et al., 2006).

160 The tropospheric nitrogen oxide family ( $\text{NO}_x = \text{NO} + \text{NO}_2$ ) participates in both OH production (reaction of nitrogen oxide (NO) with hydroperoxyl radical ( $\text{HO}_2$ ) or organic peroxy radicals ( $\text{RO}_2$ )) and loss (mainly reaction of  $\text{NO}_2$  with OH). In the Dynamically Simple Model of Atmospheric Chemical Complexity (DSMACC) used in this study (see section 2.3), the  $\text{NO}_x$  family is constrained by either  $\text{NO}_2$  or NO concentrations. We constrain the spatial distributions of boundary layer  $\text{NO}_x$  family use  
165 satellite observations of  $\text{NO}_2$  tropospheric column density use the Quality Assurance for Essential Climate Variables (QA4ECV) OMI  $\text{NO}_2$  retrieval product (Boersma et al., 2018). Due to its short lifetime,  $\text{NO}_x$  emitted from the surface mainly remains within the planetary boundary layer. Thus, satellite-retrieved vertical column densities are widely used in understanding the  $\text{NO}_2$  distributions within the boundary layer instead of the whole troposphere (e.g., Cooper et al., 2020; Geddes et al.,  
170 2017).

We also constrain tropospheric CO,  $\text{CH}_4$ , and  $\text{CH}_2\text{O}$  to better represent OH loss in the troposphere. Distributions of CO and  $\text{CH}_2\text{O}$  are taken from 4D variational data assimilation of tropospheric CO column retrieved from the spaceborne Measurements Of Pollution In The Troposphere instrument v7  
175 TIR-NIR product (MOPITT v7, Deeter et al., 2017) and column  $\text{CH}_2\text{O}$  OMI version product (OMI version3, González Abad et al. 2015), respectively (Zheng et al., 2019).  $\text{CH}_4$  distributions are taken from data assimilation of surface  $\text{CH}_4$  observations (Zhao et al., 2020a) mainly from the U.S. National Oceanic and Atmospheric Administration (NOAA/ESRL, Dlugokencky et al. (1994)). The assimilated surface CO concentration and  $\text{CH}_4$  profiles show good agreement with independent ground-based  
180 observations and aircraft observations, respectively (Zheng et al., 2019; Zhao et al., 2020a).



185 Meteorological conditions, mainly water vapor ( $\text{H}_2\text{O}_{(\text{g})}$ ) and air temperature ( $T_a$ ) can also influence tropospheric [OH]. The  $\text{H}_2\text{O}_{(\text{g})}$  (represented as specific humidity) and  $T_a$  are constrained by the second Modern-Era Retrospective analysis for Research and Applications (MERRA-2) reanalysis data from NASA's Global Modeling and Assimilation Office (GMAO) (Gelaro et al. 2017).

## 2.2 The 3D atmospheric chemistry model simulations

190 The 3D distributions of OH fields and OH precursors for the year 2010 are taken from the REF-C1 experiment of the IGAC/SPARC Chemistry-Climate Model Initiative Phase-1 (CCMI-1) (Hegglin and Lamarque, 2015; Morgenstern et al., 2017). The REF-C1 experiment is driven by state-of-the-art historical forcings and sea surface temperatures from observations and covers 51 years (1960-2010).

We include simulations from two models with different chemical mechanisms: (i) the Community Earth System Model (CESM) using the Community Atmosphere Model version 4 as atmosphere component  
195 (CESM1 CAM4-chem, Tilmes et al., 2015; 2016) and (ii) the GEOS-5 Chemistry Climate Model (GEOSCCM; Molod et al., 2012,2015; Oman et al., 2011, 2013). The tropospheric chemistry of CESM1 CAM4-chem is based on MOZART-4 mechanisms with minor updates (Emmons et al., 2010; Lamarque et al., 2012) and the GEOSCCM is based on the Global Modeling Initiative (GMI) chemistry and transport model (Duncan et al., 2007), which was originally developed for the GEOS-Chem model. The  
200 CO,  $\text{NO}_2$ ,  $\text{O}_3$ ,  $\text{CH}_4$ ,  $\text{CH}_2\text{O}$  mixing ratios, total columns  $\text{O}_3$ , and metrological conditions including  $T_a$  and  $\text{H}_2\text{O}_{(\text{g})}$  simulated by CESM1 CAM4-chem and GEOSCCM in 2010 are compared with the observational data described in Section 2.1 in the supplementary (Fig. S1, S2, and S3). A detailed description of the two model settings related to OH and the CCMI-1 model experiments can be found in Morgenstern et al. (2017) and Zhao et al. (2019).



205

### 2.3 The chemical box model DSMACC

Differing from 3D atmospheric chemistry models, which simulate the [OH] by gridded emissions inventories of its precursors, a chemical box model simulates [OH] by prescribing precursor concentrations and the meteorological states. Thus, one can estimate the sensitivity of [OH] to different precursor concentrations and meteorological parameters. Here we use the Dynamically Simple Model of Atmospheric Chemical Complexity (DSMACC; Emmerson and Evans, 2009) to estimate the sensitivity of [OH] to chemical species including CO, NO<sub>2</sub>, O<sub>3</sub>, CH<sub>4</sub>, CH<sub>2</sub>O, the total column O<sub>3</sub>, and meteorological conditions including T<sub>a</sub> and H<sub>2</sub>O<sub>(g)</sub> following the approach of Nicely et al. (2018).

The DSMACC model takes advantage of the chemical pre-processor (KPP) to generate the FORTRAN code for a chosen chemical mechanism. In this study, the DSMACC model is compiled with MOZART-4 and GEOS-Chem chemical mechanisms, respectively, to be consistent with the associated 3D models CESM1 CAM4-chem and GEOSCCM. The clear-sky photolysis rates of chemical species are estimated by the tropospheric ultraviolet and visible (TUV) radiation model. Forced by meteorological variables (H<sub>2</sub>O<sub>(g)</sub>, T<sub>a</sub>, and pressure), total column O<sub>3</sub>, and gas concentrations simulated by the CESM1 CAM4-chem and GEOSCCM, DSMACC run forward until reaching the diurnal steady state of OH. Nicely et al. (2018) have estimated the response of [OH] to changes in OH precursors by conducting DSMACC model simulations for broad latitude and pressure bins. Here we run the DSMACC model for each model pixel of the 3D grid to better represent the heterogeneous spatial distributions of OH. For example, the CESM1 CAM4-chem has 144 (longitude) × 96 (latitudes) × 13 (pressure level) model grids in the troposphere. For each sensitivity experiment (Sect. 2.4), we therefore conduct 179,712 DSMACC model simulations (for CESM1 CAM4-chem grid) each month.



## 2.4 DSMACC experiments

230 Table 1 lists the experiments conducted with the DSMACC chemical box model. The reference  
experiment (Ref\_model in Table 1) is conducted by running DSMACC with the monthly mean chemical  
species concentrations and meteorological conditions simulated by the 3D models (CESM1 CAM4-  
chem/ GEOSCCM) for each pixel using the corresponding chemical mechanisms. In the All\_obs  
simulation, the CO, NO<sub>2</sub>, O<sub>3</sub>, CH<sub>4</sub>, and CH<sub>2</sub>O, total column O<sub>3</sub>, T<sub>a</sub>, and H<sub>2</sub>O(g) are replaced with the  
235 available observational-based data (regrid to model resolution) as described in Section 2.2, while other  
DSMACC inputs (pressure and other chemical species) are the same as in Ref\_model. The observation-  
based [OH] ([OH]<sub>obs</sub>) in each 3D model pixel for two different chemical mechanisms is estimated by  
correcting [OH] as simulated by the corresponding 3D models ([OH]<sub>model</sub>) by the ratio between [OH]  
simulated by DSMACC experiments for the All\_obs ([OH]<sub>DSMACC\_all\_obs</sub>) and for the Ref\_model  
240 ([OH]<sub>DSMACC\_Ref\_model</sub>):

$$[OH]_{obs} = [OH]_{model} \times \frac{[OH]_{DSMACC\_all\_obs}}{[OH]_{DSMACC\_Ref\_model}} \quad (1)$$

Then, we also perform 8 sensitivity experiments (xk\_obs in Table 1) that only adjust one individual  
245 chemical species or meteorological condition (here and after represented as  $x_k$ ) to the observations (obs),  
keeping the other parameters equal to the simulated values from the chemistry-climate model. Because  
of high computing costs, we conduct the sensitivity experiments using only CESM1 CAM4-chem  
outputs. The OH biases due to each factor ( $\delta[OH]_k$ ) are estimated by introducing the [OH] simulated in  
the sensitivity experiment xk\_obs ([OH]<sub>DSMACC\_xk\_obs</sub>) as:

250

$$[OH]_{DSMACC\_xk\_obs} = [OH]_{model} \times \frac{[OH]_{DSMACC\_xk\_obs}}{[OH]_{DSMACC\_Ref\_model}} \quad (2)$$

$$\delta[OH]_{xk} = [OH]_{model} - [OH]_{DSMACC\_xk\_obs} \quad (3)$$



## 2.5 Chemical loss of CH<sub>4</sub>

255 We estimate the yearly tropospheric chemical loss of CH<sub>4</sub> through reaction with OH ( $L_{CH_4+OH}$ ) at global and regional scale from 2000 to 2009 by integrating the reaction of CH<sub>4</sub> with OH:

$$L_{CH_4+OH} = \sum_i \sum_t K(T) m(CH_4) [OH] \delta t \quad (4)$$

Where  $i$  is the index of the model pixel and  $\delta t$  is the integration time step (3 hours). The monthly 3D distributions of CH<sub>4</sub> mass ( $m(CH_4)$ ) during 2000-2009 are from data assimilation of surface CH<sub>4</sub> observations from NOAA/ESRL (Dlugokencky et al. 1994) and the  $T_a$  distributions are from MERRA-2 reanalysis data (see Section 2.2). The reaction rate  $K(T_a)$  is a function of  $T_a$  as given by Sander et al. (2011):

$$K(T_a) = 2.45 \times 10^{-12} e^{-\frac{1775}{T_a}} \quad (5)$$

The contribution of each factor  $x_k$  to the bias in  $\delta L_{CH_4+OH_{xk}}$  can be estimated as:

265 
$$\delta L_{CH_4+OH_{xk}} = \sum_i \sum_t K(T) m(CH_4) \delta [OH]_{xk} \delta t \quad (6)$$

With  $L_{CH_4+OH}$ , we further estimate the CH<sub>4</sub> lifetime to reaction with tropospheric OH ( $\tau_{CH_4}$ ) through the global CH<sub>4</sub> burden:

$$\tau_{CH_4} = \frac{\sum_i m(CH_4)}{L_{CH_4+OH}} \quad (7)$$

## 270 3 Results

### 3.1 Observation-based tropospheric [OH]

#### 3.1.1 Global tropospheric OH burden.

The global air-mass-weighted tropospheric mean [OH] ( $[OH]_{\text{trop-M}}$ ) simulated by CESM1 CAM4-chem and GEOSCCM in 2010 are  $11.9 \times 10^5$  molec cm<sup>-3</sup> and  $12.6 \times 10^5$  molec cm<sup>-3</sup>, respectively. By adjusting OH precursors and meteorological conditions (total column O<sub>3</sub>, tropospheric O<sub>3</sub>, CO, CH<sub>4</sub>, CH<sub>2</sub>O, boundary layer NO<sub>2</sub>, H<sub>2</sub>O<sub>(g)</sub>, and  $T_a$ ) to the observations using the DSMACC model, we estimated the



observation-based  $[\text{OH}]_{\text{trop-M}}$  to be  $9.9 \times 10^5 \text{ molec cm}^{-3}$  and  $10.4 \times 10^5 \text{ molec cm}^{-3}$  with CESM1 CAM4-chem and GEOSCCM chemical mechanisms, respectively (Fig.1 and Table 2). Compared with the original OH fields simulated by CESM1 CAM4-chem and GEOSCCM, the observation-based OH fields reduce the model-simulated global  $[\text{OH}]_{\text{trop-M}}$  by  $\sim 2 \times 10^5 \text{ molec cm}^{-3}$ . The global  $[\text{OH}]_{\text{trop-M}}$  estimated by the observation-based OH fields in this study is lower than the value estimated by Spivakovsky et al. (2000) ( $11.6 \times 10^5 \text{ molec cm}^{-3}$ ; S2000 OH field), which is used in the chemistry-transport model (CTM) intercomparison experiment (TransCom-CH4) (Patra et al., 2011) but consistent with those estimated by MCF-based inversions ( $\sim 10 \times 10^5 \text{ molec cm}^{-3}$ ; Bousquet et al., 2005; Korl and Lelieveld, 2003). The consistency with the MCF-based estimates indicates that our approach (correcting model bias through available observations) is capable of capturing the global OH burden.

### 3.1.2 The OH spatial distribution.

Fig. 1 and Fig. 2 show the spatial distribution and zonal average of the  $[\text{OH}]_{\text{trop-M}}$ , respectively, estimated from the observation-based and original model simulated OH fields. The observation-based OH fields show similar spatial distributions as their respective original model simulations, with high  $[\text{OH}]_{\text{trop-M}}$  ( $10\text{-}15 \times 10^5 \text{ molec cm}^{-3}$ ) over East Asia, South Asia, and Northern Africa, corresponding to the regions with high tropospheric  $\text{O}_3$ ,  $\text{NO}_2$ , and  $\text{H}_2\text{O}_{(\text{g})}$  (Fig. S1 and Fig. S3 ). The lowest  $[\text{OH}]_{\text{trop-M}}$  is found over the high latitudes ( $< 4 \times 10^5 \text{ molec cm}^{-3}$ ) due to less ultraviolet radiation and over the Amazon forest ( $4\text{-}8 \times 10^5 \text{ molec cm}^{-3}$ ) due to high biogenic non-methane volatile organic compounds (NMVOC) emissions. The observation-based  $[\text{OH}]_{\text{trop-M}}$  averaged over the northern tropics ( $0\text{-}30^\circ\text{N}$ ) and northern mid-to-high latitudes ( $30\text{-}90^\circ\text{N}$ ) are  $> 14 \times 10^5 \text{ molec cm}^{-3}$  and  $> 7 \times 10^5 \text{ molec cm}^{-3}$ , respectively, for both chemical mechanisms, which are higher than those over the southern tropics ( $12.2\text{-}13.6 \times 10^5 \text{ molec cm}^{-3}$ )



and southern mid-to-high-latitudes ( $5.3\text{--}5.6 \times 10^5 \text{ molec cm}^{-3}$ , Table 3 and Fig. 2). The two observation-  
300 based OH fields show similar mean [OH] over most of the latitudinal bands except for the southern  
tropics ( $0\text{--}30^\circ\text{S}$ ), where the mean  $[\text{OH}]_{\text{trop-M}}$  estimated by the GEOSCCM chemical mechanism is  $1.4 \times$   
 $10^5 \text{ molec cm}^{-3}$  higher than the one from CESM1 CAM4-chem (Table 3 and Fig. 2).

Compared to the original  $[\text{OH}]_{\text{trop-M}}$  simulated by CESM1 CAM4-chem and GEOSCCM, adjusting to  
305 observations reduces the  $[\text{OH}]_{\text{trop-M}}$  by  $2\text{--}8 \times 10^5 \text{ molec cm}^{-3}$  over most regions except the tropical forests.  
The reduction of mean  $[\text{OH}]_{\text{trop-M}}$  over the northern tropics ( $0^\circ\text{--}30^\circ\text{N}$ ) and mid-to-high latitudes ( $30^\circ\text{--}$   
 $90^\circ\text{N}$ ) are  $>3 \times 10^5 \text{ molec cm}^{-3}$  and  $>2 \times 10^5 \text{ molec cm}^{-3}$ , respectively, which is larger than that over the  
southern tropics ( $0^\circ\text{--}30^\circ\text{S}$ , by  $\sim 2 \times 10^5 \text{ molec cm}^{-3}$ ) and mid-to-high latitudes ( $30^\circ\text{--}90^\circ\text{S}$ , by  $0.6 \times 10^5$   
 $\text{ molec cm}^{-3}$ ). The Northern Hemisphere to Southern Hemisphere (N/S) ratios of the simulated OH fields  
310 are reduced from 1.35 to 1.24 for CESM1 CAM4-chem, and 1.26 to 1.15 for GEOSCCM. Although the  
N/S ratios of the observation-based OH fields are still higher than the 1, which is obtained from MCF-  
based inversions (Bousquet et al., 2005; Patra et al., 2014), incorporating available observations has  
significantly reduced the model simulated N/S ratio.

315 The spatial distribution of the observation-based [OH] of this study is different from the S2000 OH field.  
The S2000 OH field shows a high  $[\text{OH}]_{\text{trop-M}}$  over the regions with biomass burning emissions (Fig. S4).  
Instead of considering the detailed spatial distributions of nitrogen oxides, Spivakovsky et al. (2000) use  
a series of  $\text{NO}_t$  ( $\text{NO}_2 + \text{NO} + 2\text{N}_2\text{O}_5 + \text{NO}_3 + \text{HNO}_2 + \text{HNO}_4$ ) profiles for land and ocean over large regions  
(Fig. S5). As shown in Fig. S4 and Fig. S5, the highest  $[\text{OH}]_{\text{trop-M}}$  over South America and Africa  
320 estimated by Spivakovsky et al. (2000) correspond to high  $\text{NO}_t$  mixing ratios over these two regions.  
The [OH] shows high positive sensitivity to  $\text{NO}_t$  in the free troposphere, due to low VOCs and  $\text{NO}_t$   
mixing ratios (Fig. S6). Using satellite observations, Choi et al. (2014) showed that the high  $\text{NO}_2$  mixing



ratios in the free troposphere are mainly located near polluted urban regions (e.g., North America, Europe, and Asia), which is more similar to the  $\text{NO}_2$  distribution simulated by 3D atmospheric models (Fig. S1). Thus, although the S2000 OH field gives an N/S ratio of 1, its spatial distribution may have biases due to the simplification in the  $\text{NO}_t$  distributions.

### 3.2 Contribution from individual factors to model biases in $[\text{OH}]_{\text{trop-M}}$

By conducting the sensitivity simulations listed in Table 1, we estimate the contribution of individual factors to model biases based on Equation 2-3. The sensitivity of OH to model biases in tropospheric  $\text{O}_3$ , stratospheric  $\text{O}_3$ ,  $\text{H}_2\text{O}_{(\text{g})}$ , and  $\text{NO}_x$  emissions have been tested in Strode et al. (2015) using GEOSCCM. In this Section, we extend the procedure of Strode et al. (2015) by including more factors:  $T_a$ , CO,  $\text{CH}_2\text{O}$ ,  $\text{CH}_4$ , and  $\text{NO}_2$  in the boundary layer.

Table 4 summarizes the contribution of each chemical precursor and meteorological condition to the difference between CESM1 CAM4-chem simulated and observation-based global  $[\text{OH}]_{\text{trop-M}}$ . The total contribution of the 8 individual factors to the difference in global  $[\text{OH}]_{\text{trop-M}}$  estimated from the simulation  $xk_{\text{obs}}$  is  $2.0 \times 10^5 \text{ molec cm}^{-3}$  (Table 4), consistent with that estimated from the simulation All\_obs (Table 2), indicating that the nonlinear effect of atmospheric chemistry is negligible on the global scale. Indeed, although the atmospheric OH is produced and removed through complex nonlinear chemical reactions, one can infer the large-scale  $[\text{OH}]_{\text{trop-M}}$  changes by roughly summing the influence from individual factors.

#### 3.2.1 Contribution from CO

CO is the largest OH sink in the troposphere (Lelieveld et al., 2016; Zhao et al., 2020b). The sensitivity simulation CO\_obs shows that a 1 ppbv increase in CO can result in a decrease in [OH] by up to more



than  $3 \times 10^4$  molec  $\text{cm}^{-3}$  (Fig. S6). Compared with the CO distributions from inversions that assimilated MOPITT observations, the CESM1 CAM4-chem underestimates the global tropospheric mean CO mixing ratio by 24 ppbv (Fig. S1). Based on the DSMACC simulations CO\_obs and Ref\_CESM (Table 1), we find that the negative bias in CO contributes most to the difference in the modeled versus observation-based  $[\text{OH}]_{\text{trop-M}}$  ( $1.3 \times 10^5$  molec  $\text{cm}^{-3}$ ; Table 4 and Figure 3). The underestimation of CO is common in atmospheric models and was treated either as a cause or an effect of the overestimated  $[\text{OH}]$  in previous studies (Naik et al., 2013; Monks et al. 2015; Stode et al., 2015). For example, based on the ACCMIP simulations, Naik et al. (2013) found that the positive bias in  $[\text{OH}]$  was most likely due to the underestimation of CO when compared with both satellite and surface observations. In contrast, Strode et al. (2015) did sensitivity simulations using the GEOSCCM model and showed that reducing OH bias could improve the accuracy of modeled CO. In this study, we do not intend to solve the cause/effect issue between CO and OH, since the discrepancy in  $[\text{OH}]_{\text{trop-M}}$  of  $1.3 \times 10^5$  molec  $\text{cm}^{-3}$  could also be understood as the global tropospheric  $[\text{OH}]$  changes that would be needed to simulate the observed CO.

The underestimation of the CO mixing ratio is larger over the Northern Hemisphere (30 ppbv) than over the Southern Hemisphere (18 ppbv) (Fig.S1). The largest bias in  $[\text{OH}]_{\text{trop-M}}$  induced by CO is found over the northern tropics ( $1.9 \times 10^5$  molec  $\text{cm}^{-3}$ ) followed by those over the northern mid-to-high latitude regions and the southern tropics ( $1.2 \times 10^5$  molec  $\text{cm}^{-3}$ ; Table 4 and Fig. 2). Naik et al. (2013) demonstrated that the model bias in CO contributes to the overestimation of the modeled N/S ratio in  $[\text{OH}]_{\text{trop-M}}$ . In this study, although the underestimation of CO leads to a larger positive bias of  $[\text{OH}]_{\text{trop-M}}$  over the Northern Hemisphere than the Southern Hemisphere, the observation-based adjustment only reduces the positive bias of the N/S ratio by 0.02. This means that the N/S difference of the CO bias is not sufficient to explain the inconsistency between the CESM1 CAM4-chem simulated and MCF-based N/S ratio in  $[\text{OH}]_{\text{trop-M}}$ .



### 3.2.2 Contribution from tropospheric O<sub>3</sub>

Tropospheric O<sub>3</sub> can contribute to both primary and secondary OH production. Compared to satellite observations from OMI, CESM1 CAM4-chem simulations show a large overestimation of tropospheric O<sub>3</sub> over the 15-60°N (up to 14 DU, 40%) and an underestimation (14 DU, 40%) over the tropics and Southern Hemisphere (Fig. S1).

At the global scale, the model bias in O<sub>3</sub> leads to a negative bias on [OH]<sub>trop-M</sub> by  $0.3 \times 10^5$  molec cm<sup>-3</sup>, much smaller than that caused by CO (Table 4). However, at the regional scale, The CESM1 CAM4-chem simulated [OH]<sub>trop-M</sub> is enhanced by  $\sim 1 \times 10^5$  molec cm<sup>-3</sup> over the tropics (15°S-15°N) and  $\sim 0.5 \times 10^5$  molec cm<sup>-3</sup> over the mid-southern hemisphere (15°-60°S), while it is reduced by  $0.1-0.3 \times 10^5$  molec cm<sup>-3</sup> over the mid-northern hemisphere (15°-60°N) when adjusted to OMI/MLS tropospheric column O<sub>3</sub> (Fig. 2). The adjustment reduces the N/S ratio of [OH]<sub>trop-M</sub> by 0.07, still cannot explain the overestimation of the N/S ratio but leads to a larger correction than the one with CO alone.

### 3.2.3 Contribution from boundary layer NO<sub>2</sub>.

The sensitivity of OH to NO<sub>2</sub> is highly variable. We estimate that a 1 ppbv increase in NO<sub>2</sub> can lead to a change of [OH] ranging from  $-3 \times 10^6$  molec cm<sup>-3</sup> to more than  $+10 \times 10^6$  molec cm<sup>-3</sup>, depending on the mixing ratio of NMVOCs (represented as HCHO+isoprene) and NO<sub>2</sub> (Fig. S6). Compared to the QA4ECV NO<sub>2</sub> retrieval product, CESM CAM-Chem overestimates tropospheric NO<sub>2</sub> over most regions except North China and tropical forests (Fig. S1).



At the global scale, the overestimation of  $\text{NO}_2$  leads to a positive bias in  $[\text{OH}]_{\text{trop-M}}$  by  $0.3 \times 10^5$  molec  $\text{cm}^{-3}$  (Table 4). At the regional scale, correcting for the PBL  $\text{NO}_2$  does not influence the N/S ratio of OH. As shown in Fig. 3, the overestimation of PBL  $\text{NO}_2$  results in positive bias in  $[\text{OH}]_{\text{trop-M}}$  over most of the continental regions. Over tropical and temperate oceans, one can also see that the slight overestimation in  $\text{NO}_2$  leads to a significant positive bias in OH by  $0.5\text{--}1 \times 10^5$  molec  $\text{cm}^{-3}$  since the sensitivity of  $[\text{OH}]_{\text{trop-M}}$  to  $\text{NO}_2$  can be very high ( $10^7$  molec  $\text{cm}^{-3}/$  ppbv  $\text{NO}_2$ ) over the regions with low  $\text{NO}_x$  and NMVOC mixing ratios. Over North China, although the model shows a large underestimation in  $\text{NO}_2$  (Fig.S1), the  $[\text{OH}]_{\text{trop-M}}$  is slightly smaller after adjustment. This is because over high  $\text{NO}_2$  regions, the [OH] is not sensitive to an increase in  $\text{NO}_2$  or even shows a negative response (Fig. S6).

### 3.2.4 Contribution from total column $\text{O}_3$

The total column  $\text{O}_3$  mainly influences  $\text{O}^1(\text{D})$  photolysis through absorbing UV radiation. The CESM1 CAM4-chem mainly underestimates the total  $\text{O}_3$  columns by up to  $\sim 10$  DU over tropical regions compared with the SBUV/MOD observations (Fig. S2). On a global scale, the underestimation of the  $\text{O}_3$  total column can lead to an overestimation of the  $[\text{OH}]_{\text{trop-M}}$  by  $\sim 0.6 \times 10^5$  molec  $\text{cm}^{-3}$  (Fig. 2 and Fig. 3), comparable with that due to tropospheric  $\text{O}_3$ .

### 3.2.5 Contribution from $\text{CH}_4$ and $\text{CH}_2\text{O}$

In CCMI-1 simulations, atmospheric chemistry models prescribe the lower boundary conditions for  $\text{CH}_4$  following the Representative Concentration Pathway (RCP6.0). Compared to the posterior  $\text{CH}_4$  fields from inversions by assimilating the surface  $\text{CH}_4$  observations, the tropospheric mean  $\text{CH}_4$  mixing ratios used in the CESM CAM4-chem are  $\sim 80$  ppbv lower over the tropical and extratropical regions with high biomass burning and anthropogenic emissions, and  $\sim 40$  ppbv lower over other regions. But due to



the low sensitivity of [OH] to CH<sub>4</sub> changes (Fig. S1), the underestimation in CH<sub>4</sub> only leads to a small positive bias in the global tropospheric mean [OH] by  $0.1 \times 10^5$  molec cm<sup>-3</sup>.

420 CESM CAM4-chem overestimates CH<sub>2</sub>O by more than 50% over land but slightly underestimates CH<sub>2</sub>O over tropical oceans (Fig.S1). Since the CH<sub>2</sub>O contributes to only a small part (6%) of the total [OH] loss (Zhao et al., 2020b), such a large bias in the CESM CAM4-Chem simulated CH<sub>2</sub>O only leads to a small positive bias global mean [OH]<sub>trop-M</sub> by  $0.1 \times 10^5$  molec cm<sup>-3</sup> (Fig.3).

### 3.2.6 Contribution from meteorological conditions

425 H<sub>2</sub>O<sub>(g)</sub> is a major OH precursor that contributes to the primary production of OH and T<sub>a</sub> can influence OH production and loss rates. Compared to MERRA2 reanalysis data, CESM CAM4-chem overestimates zonally averaged H<sub>2</sub>O<sub>(g)</sub> mixing ratios near the surface and around 800 hPa by ~1.5g/kg (Fig. S3). The sensitivity experiments show that a change in specific humidity by 1g/kg can lead to a change in [OH] by  $>3 \times 10^5$  molec cm<sup>-3</sup> over the regions with high O(<sup>1</sup>D) photolysis and low NMVOC  
430 mixing ratios (Fig. S6). As shown in Table 4 and Fig.3, globally, the model bias in H<sub>2</sub>O<sub>(g)</sub> only leads to a small bias ( $0.1 \times 10^5$  molec cm<sup>-3</sup>) in [OH]<sub>trop-M</sub>, but regionally, the model bias in H<sub>2</sub>O<sub>(g)</sub> can lead to a bias in [OH]<sub>trop-M</sub> by the magnitude of  $5.0 \times 10^5$  molec cm<sup>-3</sup>, even larger than that induced by the bias in CO. For T<sub>a</sub>, the model only shows a small bias (<1°C) compared with MERRA2 reanalysis data (Fig. S3). Thus, model bias in [OH]<sub>trop-M</sub> induced by T<sub>a</sub> is negligible (Fig. 4).

## 3.3 Chemical sinks of CH<sub>4</sub> as estimated by observation-based OH fields

### 3.3.1 Global and regional OH chemical sink of CH<sub>4</sub>



Using the observation-based OH field, we estimate that the global tropospheric CH<sub>4</sub> loss by reaction with tropospheric OH ( $L_{\text{CH}_4+\text{OH}}$ ) averaged during the period 2000 through 2009 is 434 Tg yr<sup>-1</sup> and 461 Tg yr<sup>-1</sup> for CESM1 CAM4-chem and GEOSCCM, respectively. These estimates are about 105 Tg yr<sup>-1</sup> lower than estimated by the original model simulated OH fields (540 Tg yr<sup>-1</sup> and 565 Tg yr<sup>-1</sup>, respectively; Table 2). The corresponding CH<sub>4</sub> lifetimes against tropospheric OH loss estimated by the two observation-based OH fields are 11.4 yr and 10.7 yr for CESM1 CAM4-chem and GEOSCCM, respectively, well within the range estimated by Prather et al. (2012) based on the MCF-inversions (11.2 ± 1.3yr) and much longer than estimated by the original model simulated OH fields (9.1 yr for CESM1 CAM4-chem and 8.7 yr for GEOSCCM).

As shown in Table 3, more than 70% of the tropospheric  $L_{\text{CH}_4+\text{OH}}$  occurs over tropical regions mainly due to both high [OH] and  $T_a$ . Constraining the tropospheric [OH] by precursor concentrations reduces the tropospheric  $L_{\text{CH}_4+\text{OH}}$  by ~30 Tg yr<sup>-1</sup> (16%) over the southern tropics, ~50 Tg yr<sup>-1</sup> (21%) over the northern tropics, and ~25 Tg yr<sup>-1</sup> (25%) over the northern mid-to-high latitude as estimated by both CESM1 CAM4-chem and GEOSCCM OH fields. Over the southern mid-to-high latitude regions, there are only a few changes (6 Tg yr<sup>-1</sup>) in tropospheric  $L_{\text{CH}_4+\text{OH}}$ . Thus, constraining tropospheric [OH] by precursor concentrations changes the inter-hemispheric distribution of  $L_{\text{CH}_4+\text{OH}}$ . The values of  $L_{\text{CH}_4+\text{OH}}$  estimated by the observation-based OH fields are ~35 Tg yr<sup>-1</sup> and ~75 Tg yr<sup>-1</sup> lower than that estimated by the corresponding original model simulated OH fields over the Southern and Northern Hemispheres, respectively (Table 3). Thus, the inter-hemispheric difference of  $L_{\text{CH}_4+\text{OH}}$  (north – south) estimated by observation-based OH fields (60 Tg yr<sup>-1</sup> by CESM1 CAM4-chem and 48 Tg yr<sup>-1</sup> by GEOSCCM) is ~40% lower than estimated by the original model simulated OH fields (98 Tg yr<sup>-1</sup> by CESM1 CAM4-chem and 81 Tg yr<sup>-1</sup> by GEOSCCM).



### 3.3.2 Global total chemical sink of CH<sub>4</sub>

We estimate the global total CH<sub>4</sub> chemical sink for 2000-2009 by gathering: (1) the tropospheric L<sub>CH<sub>4</sub>+OH</sub> estimated using the original model-simulated and observation-based OH fields, (2) the CH<sub>4</sub> loss in the stratosphere (26 Tg yr<sup>-1</sup> estimated by CESM1 CAM4-chem and 36 Tg yr<sup>-1</sup> estimated by GEOSCCM simulations) and CH<sub>4</sub> oxidated by chlorine (11 Tg yr<sup>-1</sup>) given by Saunois et al. (2020). We then compare the chemical sink estimated in this study with that estimated by the bottom-up and top-down methods given by previous GCP global CH<sub>4</sub> budget (Saunois et al., 2016; 2020).

As shown in Fig. 4, the bottom-up estimates in the GCP global CH<sub>4</sub> budget (blue bars) have a large range (483-738 Tg yr<sup>-1</sup> in Saunois et al. (2016) and 489-779 Tg yr<sup>-1</sup> in Saunois et al. (2020)), much higher than those from the top-down method (514 Tg yr<sup>-1</sup> in Saunois et al. (2016) and 459-516 Tg yr<sup>-1</sup> in Saunois et al. (2020)). The CH<sub>4</sub> sinks simulated by CESM1 CAM4-chem (549 Tg yr<sup>-1</sup>) and GEOSCCM (585 Tg yr<sup>-1</sup>) were included in the bottom-up estimates in Saunois et al. (2020) (green bar) and is slightly lower than the average value estimated using different OH fields (595 Tg yr<sup>-1</sup>).

In this study, the global total CH<sub>4</sub> chemical sinks estimated using the originally simulated tropospheric OH and constrained CH<sub>4</sub> mixing ratios are 577 Tg yr<sup>-1</sup> and 612 Tg yr<sup>-1</sup> for CESM1 CAM4-chem and GEOSCCM, respectively, close to the mean values estimated by the bottom-up method (around 600 Tg yr<sup>-1</sup>) using different OH fields but much higher than the top-down estimates (around 500 Tg yr<sup>-1</sup>). It should be noted that the bottom-up estimates of the chemical loss of CH<sub>4</sub> in previous GCP global CH<sub>4</sub> budget were calculated using model-simulated CH<sub>4</sub> mixing ratios (Fig.4; Saunois et al. 2020). The CH<sub>4</sub> mixing ratios simulated by CESM1 CAM4-chem and GEOSCCM are lower than that used in this study (Fig. S1). Thus, the chemical sink of CH<sub>4</sub> estimated in this study is higher than that estimated in Saunois et al. (2020) by ~30 Tg yr<sup>-1</sup>. After adjusting the main OH precursors to observations, the global



chemical sink of CH<sub>4</sub> is 471-508 Tg yr<sup>-1</sup>, as estimated using the two observation-based OH fields, more consistent with top-down method estimates (~500Tg yr<sup>-1</sup>).

The above analyses show that the large uncertainties in the bottom-up estimates of the CH<sub>4</sub> chemical sink are attributable to the use of the model-simulated OH fields with known biases. Constraining the OH field with available precursor observations to correct the global [OH], the magnitude of the methane loss is more in line with top-down methane inversions. Therefore, we partly reconcile the bottom-up and top-down estimates of the CH<sub>4</sub> sink. Although only two of seven bottom-up models synthesized in Saunio et al. (2020) are considered in this study, our approach can be generalized to other chemistry-climate models. Instead of directly using the OH fields simulated from an atmospheric chemistry model, the bottom-up estimates can use the precursor observations and box-model based approach proposed here to reduce model biases of OH fields.

### 3.3.3 Contribution from the model biases of individual OH precursors to chemical sink of CH<sub>4</sub>

We further quantify the influence of model biases in individual OH precursors on the bottom-up estimates of CH<sub>4</sub> chemical sink ( $\delta L_{\text{CH}_4+\text{OH}_{\text{Xk}}}$ ). At the global scale, the underestimation of CO and total column O<sub>3</sub> and the overestimation of NO<sub>2</sub> by the CESM1 CAM4-chem lead to a positive bias of 60 Tg yr<sup>-1</sup> (11%), 22 Tg yr<sup>-1</sup> (4%), and 22 Tg yr<sup>-1</sup> (4%) in tropospheric L<sub>CH<sub>4</sub>+OH</sub> (Fig.4 and Table 4), respectively, while an underestimation of tropospheric O<sub>3</sub> leads to a negative bias of 17 Tg yr<sup>-1</sup> (3%) in tropospheric L<sub>CH<sub>4</sub>+OH</sub>. Although the model bias of [OH]<sub>trop-M</sub> induced by H<sub>2</sub>O<sub>(g)</sub> is negligible on the global scale, the observation-based adjustment of H<sub>2</sub>O<sub>(g)</sub> leads to a reduction in tropospheric L<sub>CH<sub>4</sub>+OH</sub> by 10 Tg (2%), since the model overestimation of H<sub>2</sub>O<sub>(g)</sub> is concentrated over the mid-to-low latitude regions where tropospheric CH<sub>4</sub> oxidation mainly occurs (Fig. S3). The model bias in CH<sub>2</sub>O and CH<sub>4</sub> itself leads to a small positive bias of ~1% respectively on L<sub>CH<sub>4</sub>+OH</sub>.



510

As the tropospheric  $L_{\text{CH}_4+\text{OH}}$  mainly occurs over the mid-to-low latitude regions, the biases in  $[\text{OH}]_{\text{trop-M}}$  over the high latitudes (north of  $60^\circ\text{N}$  or south of  $60^\circ\text{S}$ ) due to an overestimation of CO and underestimation of  $\text{H}_2\text{O}_{(\text{g})}$  (Fig. 2), do not substantively contribute to the bias in  $L_{\text{CH}_4+\text{OH}}$  (Fig. 5). Over the regions north of  $15^\circ\text{N}$ , nearly all the precursors considered in this study contribute to the overestimation of  $L_{\text{CH}_4+\text{OH}}$  (55  $\text{Tg yr}^{-1}$  in total), of which 47% (26  $\text{Tg yr}^{-1}$ ) is contributed by model underestimation of CO. South of  $15^\circ\text{N}$ , the underestimation of tropospheric  $\text{O}_3$  results in an underestimation of  $L_{\text{CH}_4+\text{OH}}$  by 22  $\text{Tg yr}^{-1}$ , partly offsetting the overestimation of  $L_{\text{CH}_4+\text{OH}}$  induced by CO (34  $\text{Tg yr}^{-1}$ ) and other precursors (40  $\text{Tg yr}^{-1}$  in total) (Fig. 5). As aforementioned, the inter-hemispheric difference of  $L_{\text{CH}_4+\text{OH}}$  derived from the observation-based OH fields is 48  $\text{Tg yr}^{-1}$  smaller than estimated using the OH field originally simulated by CESM1 CAM4-chem. The biases in CO, tropospheric  $\text{O}_3$ , and boundary layer  $\text{NO}_2$ , lead to an overestimation of the inter-hemispheric difference of tropospheric  $L_{\text{CH}_4+\text{OH}}$  by 15  $\text{Tg yr}^{-1}$ , 15  $\text{Tg yr}^{-1}$ , and 9  $\text{Tg yr}^{-1}$ , respectively, dominant the bias in the inter-hemispheric difference in tropospheric  $L_{\text{CH}_4+\text{OH}}$ .

#### 525 **4 Conclusion and discussion**

In this study, we aim to reconcile the top-down and bottom-up estimates of the global  $\text{CH}_4$  sink and to quantify the contribution of each factor to the overestimation of tropospheric  $[\text{OH}]$  that is generally found in atmospheric chemistry models and to the consequent overestimation of  $\text{CH}_4$  chemical loss in the bottom-up method. To do so, we propose a new approach based on precursor observations and a chemical box model, to improve the 3D distributions of tropospheric OH radicals issued from atmospheric chemistry models.

530



We estimate two 3D observation-based OH fields based on three components: (i) simulated tropospheric [OH] and related chemical species from global 3D atmospheric chemistry models (here CESM1-CAM4chem and GEOSCCM), (ii) the sensitivities of tropospheric [OH] to its precursors in each model grid cell estimated by the chemical box model DSMACC using a chemical mechanism similar to the 3D model, and (iii) observations of chemical species related to OH production and loss (CO, O<sub>3</sub>, boundary layer NO<sub>2</sub>, CH<sub>4</sub>, CH<sub>2</sub>O, and total column O<sub>3</sub>) and meteorological conditions (H<sub>2</sub>O<sub>(g)</sub> and T<sub>a</sub>). The chemical box model DSMACC can be compiled using different chemical mechanisms, making it possible to apply this approach to other atmospheric chemistry models and improve the OH.

The global [OH]<sub>trop-M</sub> estimated from observation-based OH fields is  $\sim 10 \times 10^5$  molec cm<sup>-3</sup> in 2010 based on two different chemical mechanisms, which is  $2 \times 10^5$  molec cm<sup>-3</sup> lower than the original model-simulated global [OH]<sub>trop-M</sub>, consequently reaching consistency with the value derived by MCF-based inversions (around  $10 \times 10^5$  molec cm<sup>-3</sup>; Bousquet et al., 2005; Korl and Lelieveld, 2003). The observation-based adjustments also change the latitudinal distribution of [OH], reducing the north to south ratios from 1.35 and 1.26 to 1.24 and 1.15 for CESM1 CAM4-chem and GEOSCCM, respectively, closer to the one obtained from MCF-based inversions (slightly smaller than 1).

Based on the simulations from CESM1 CAM4-chem, globally, the overestimation of [OH]<sub>trop-M</sub> arises mainly from the underestimation of CO and total column O<sub>3</sub>, and the overestimation of boundary layer NO<sub>2</sub>, which contribute  $1.3 \times 10^5$  molec cm<sup>-3</sup>,  $0.4 \times 10^5$  molec cm<sup>-3</sup>, and  $0.3 \times 10^5$  molec cm<sup>-3</sup>, respectively, to the bias in [OH]<sub>trop-M</sub>. For the N/S ratio of [OH]<sub>trop-M</sub>, the positive bias in [OH]<sub>trop-M</sub> over the Northern Hemisphere ( $0.1-0.3 \times 10^5$  molec cm<sup>-3</sup>) and the negative bias over the tropics and Southern Hemisphere ( $0.5-1.0 \times 10^5$  molec cm<sup>-3</sup>) due to tropospheric O<sub>3</sub> dominate the higher N/S ratio of [OH]<sub>trop-M</sub> estimated by the CESM1 CAM4-chem than the observation-based OH field. At the regional scale, the model bias



in  $\text{H}_2\text{O}_{(\text{g})}$  can lead to bias in  $[\text{OH}]_{\text{trop-M}}$  even larger than that induced by CO.

The global  $\text{CH}_4$  loss by reaction with tropospheric OH ( $L_{\text{CH}_4+\text{OH}}$ ) estimated from the observation-based OH fields is  $434 \text{ Tg yr}^{-1}$  and  $461 \text{ Tg yr}^{-1}$  for CESM1 CAM4-chem GEOSCCM, respectively, averaged over 2000 to 2009, which is lower than that estimated from the original model simulated OH fields by around  $105 \text{ Tg yr}^{-1}$ . Based on the results from CESM1 CAM4-chem, at the global scale, the underestimation of CO and total column  $\text{O}_3$ , and overestimation of  $\text{NO}_2$  lead to positive biases in tropospheric  $L_{\text{CH}_4+\text{OH}}$  by  $60 \text{ Tg yr}^{-1}$  (11%),  $22 \text{ Tg yr}^{-1}$  (4%), and  $22 \text{ Tg yr}^{-1}$  (4%), respectively, while an underestimation of tropospheric  $\text{O}_3$  leads to a negative bias in tropospheric  $L_{\text{CH}_4+\text{OH}}$  by  $17 \text{ Tg yr}^{-1}$  (3%). The inter-hemispheric difference in the tropospheric  $L_{\text{CH}_4+\text{OH}}$  is therefore reduced by 40% (around  $35 \text{ Tg yr}^{-1}$ ) when estimated using the observation-based OH field. Although the bias in the N/S ratio of  $[\text{OH}]_{\text{trop-M}}$  is dominated by the tropospheric  $\text{O}_3$  concentration, the positive bias in the inter-hemispheric difference of  $L_{\text{CH}_4+\text{OH}}$  is determined together by the biases in CO ( $15 \text{ Tg yr}^{-1}$ ), tropospheric  $\text{O}_3$  ( $15 \text{ Tg yr}^{-1}$ ), and boundary layer  $\text{NO}_2$  ( $9 \text{ Tg yr}^{-1}$ ).

Using the tropospheric  $L_{\text{CH}_4+\text{OH}}$  estimated with our observation-based OH fields, the global total  $\text{CH}_4$  chemical sink is  $471\text{-}508 \text{ Tg yr}^{-1}$ . This quantification is more consistent with top-down estimates in the previous GCP global  $\text{CH}_4$  budget ( $459\text{-}516 \text{ Tg yr}^{-1}$ , Saunois et al., 2016; 2020) than it was before the adjustment ( $577\text{-}612 \text{ Tg yr}^{-1}$ ). The bottom-up method in the previous GCP global  $\text{CH}_4$  budget estimated the  $\text{CH}_4$  chemical sink directly using the OH fields simulated by atmospheric chemistry models. However, the uncertainties in the model simulated OH lead to an unreliable range in the bottom-up estimated  $\text{CH}_4$  chemical sink, much higher than that estimated by the top-down method. Our results highlight that constraining the OH fields using available precursor observations can improve the bottom-up estimates of the  $\text{CH}_4$  sink and help reconcile the difference between the top-down and



bottom-up estimates of the CH<sub>4</sub> sink.

Although the observation-based 3D OH fields presented in this study can capture the global tropospheric OH burden and chemical loss of CH<sub>4</sub>, unresolved uncertainties remain. For example, the difference in global [OH]<sub>trop-M</sub> between the two observation-based OH fields estimated from CESM1 CAM4-chem and GEOSCCM simulations is  $0.6 \times 10^5$  molec cm<sup>-3</sup>. Such a difference is partly be attributable to their differences in chemical mechanisms. As discussed in Murray et al. (2021), the inter-model differences in tropospheric [OH] and its responses to precursors are largely determined by the oxidative efficiency of NMVOCs and the lifetime of NO<sub>x</sub> simulated by the models. Reducing the uncertainties due to the modeled chemical mechanisms relies on additional observations to improve the simulation of NMVOCs oxidative efficiency and NO<sub>x</sub> lifetime.

In addition, the data that we use to constrain the OH precursors come mainly from satellite observations and reanalysis data, of which the uncertainties are not considered in this study. For example, the MERRA-2 reanalysis data significantly overestimate H<sub>2</sub>O<sub>(g)</sub> in the upper troposphere (Jiang et al., 2015); The QA4ECV tropospheric NO<sub>2</sub> vertical column density is lower compared with surface observations under the extreme high-pollution case compared with surface observations (Compernelle et al., 2020). Therefore, the performance of this method thus depends on the accuracy of observations used to constrain individual factors. Since the sensitivity of [OH] to each precursor is estimated by the chemical box model, we can easily improve the [OH] using the updated observational datasets.

Another key factor that could influence the tropospheric OH burden but is unconstrained in this study is NO<sub>2</sub> in the free troposphere. Although the NO<sub>2</sub> mixing ratio is usually less than 1 ppbv in the free troposphere, the sensitivity of [OH] to NO<sub>2</sub> can be very high in low NO<sub>2</sub> regions. However, a potential



605 model bias due to lightning  $\text{NO}_x$  emissions, which had proven to contribute significantly to the upper-tropospheric  $[\text{OH}]$  burden (Murray et al., 2013; Turner et al., 2018), is not adjusted in our study. Satellite retrievals for upper tropospheric  $\text{NO}_2$  (e.g. Belmonte Rivas et al., 2015; Marais et al., 2021) could help quantify  $[\text{OH}]$  biases due to free tropospheric  $\text{NO}_2$  and the contribution of lightning  $\text{NO}_x$  emissions.

610 The observation-based adjustment reduces the simulated N/S ratio of  $[\text{OH}]_{\text{trop-M}}$  by 0.1 only, which is still higher than the one obtained from MCF-inversions (less than 1.0). This difference indicates that the overestimation of N/S ratio by atmospheric models cannot be fully explained by the underestimation of CO and overestimation of  $\text{O}_3$  over the Northern Hemisphere as mentioned in previous studies (Naik et al. 2013). Including the chemical mechanism such as OH recycling by isoprene (Lelieveld et al. 2008) may help further reduce the N/S ratio for model-simulated OH fields.

The new approach proposed here to improve the 3D OH fields and chemical loss of  $\text{CH}_4$  can be applicable broadly. It relies on observations of OH precursor concentrations that can be applied  
620 efficiently to any atmospheric chemistry model with a box-model (0D) available. Here we only apply this method to two models for one year (2010) and both of them agree with MCF-based inversions in terms of the global OH burden. One future research development is to generate observation-based OH fields for all the atmospheric chemistry models included in the GCP global  $\text{CH}_4$  budget and over a longer time period to see if higher consistency can also be achieved on longer timescales. It will also be  
625 important to assess how much uncertainty in  $[\text{OH}]$  means and trends can be further reduced and achieved in detail.

Also, the  $\text{CH}_4$  emissions from top-down approaches used mostly a single OH field from Spivakosky



(2000), which is climatological data without any interannual variations. Some CH<sub>4</sub>-inversions used the  
630 OH fields from chemistry-climate or chemistry-transport models with the known aforementioned biases  
that may lead to bias in the inverted surface CH<sub>4</sub> fluxes. Our OH product could be used instead in CH<sub>4</sub>  
inversions to better infer CH<sub>4</sub> emissions and reduce the uncertainties in the global methane budget.  
Further work is necessary to consider the interannual changes in our observation-based estimates.

### 635 **Data availability**

The GEOSCCM OH fields are available at the Centre for Environmental Data Analysis  
(CEDA; <http://data.ceda.ac.uk/badc/wcrp-ccmi/data/CCMI-1/output>; last access: December 2019,  
Hegglin and Lamarque, 2015), the Natural Environment Research Council's Data Repository for  
Atmospheric Science and Earth Observation. The CESM1 CAM4-chem outputs for CCMI are available  
640 at <http://www.earthsystemgrid.org> (Climate Data Gateway at NCAR, last access: December 2019).

### **Code availability**

The DSMACC model code and descriptions are available at [http://wiki.seas.harvard.edu/geos-chem/index.php/Main\\_Page](http://wiki.seas.harvard.edu/geos-chem/index.php/Main_Page).

### 645 **Author contributions**

YZ, MS, and PB designed the study, analyzed data, and wrote the manuscript. XL helped with data  
preparation. JGC and RBJ provided input into the study design and discussed the results. MIH provided  
CCMI model outputs. BZ provided the assimilated CO and CH<sub>2</sub>O distributions. All co-authors  
650 commented on the manuscript.

### **Acknowledgements**

This work benefited from and is a contribution to the Global Methane Budget activity of the Global Carbon Project.

655 We acknowledge the modeling groups for making their simulations available for this analysis, the joint WCRP SPARC/IGAC Chemistry–Climate Model Initiative (CCMI) for organizing and coordinating the model simulations and data analysis activity, and the British Atmospheric Data Centre (BADC) for collecting and archiving the CCMI model output. JGC acknowledges support from the National Environmental Science Program – Climate Systems Hub. RBJ acknowledges the U.N. Environment  
660 Programme for support of the Global Methane Budget.

### Competing interests

The authors declare that they have no conflicts of interest.

### Financial support

665 This research has been supported by Shandong Provincial Natural Science Foundation (grant no. 2022HWYQ-066) and the Gordon and Betty Moore Foundation (grant no. GBMF5439), “Advancing Understanding of the Global Methane Cycle”, and the U.N. Environment Programme.

### Reference

670 Ball, W. T., Alsing, J., Staehelin, J., Davis, S. M., Froidevaux, L., and Peter, T.: Stratospheric ozone trends for 1985–2018: sensitivity to recent large variability, *Atmos. Chem. Phys.*, 19, 12731–12748, 10.5194/acp-19-12731-2019, 2019.

Boersma, K. F., Eskes, H. J., Richter, A., De Smedt, I., Lorente, A., Beirle, S., van Geffen, J. H. G. M., Zara, M., Peters, E., Van Roozendaal, M., Wagner, T., Maasakkers, J. D., van der A, R. J., Nightingale, J., De Rudder, A., Irie, H., Pinardi, G., Lambert, J. C., and Compernolle, S. C.: Improving algorithms and uncertainty estimates for satellite NO<sub>2</sub> retrievals: results from the quality assurance for the essential climate variables (QA4ECV) project, *Atmos. Meas. Tech.*, 11, 6651–6678, 10.5194/amt-11-6651-2018,

675



2018.

680 Bousquet, P., Hauglustaine, D. A., Peylin, P., Carouge, C., and Ciais, P.: Two decades of OH variability as inferred by an inversion of atmospheric transport and chemistry of methyl chloroform, *Atmos. Chem. Phys.*, 5, 2635-2656, 10.5194/acp-5-2635-2005, 2005.

Choi, S., Joiner, J., Choi, Y., Duncan, B. N., Vasilkov, A., Krotkov, N., and Bucsela, E.: First estimates of global free-tropospheric NO<sub>2</sub> abundances derived using a cloud-slicing technique applied to satellite observations from the Aura Ozone Monitoring Instrument (OMI), *Atmos. Chem. Phys.*, 14, 10565-10588, 10.5194/acp-14-10565-2014, 2014.

685 Cooper, M. J., Martin, R. V., McLinden, C. A., and Brook, J. R.: Inferring ground-level nitrogen dioxide concentrations at fine spatial resolution applied to the TROPOMI satellite instrument, *Environmental Research Letters*, 15, 104013, 10.1088/1748-9326/aba3a5, 2020.

Deeter, M. N., Edwards, D. P., Francis, G. L., Gille, J. C., Martínez-Alonso, S., Worden, H. M., and Sweeney, C.: A climate-scale satellite record for carbon monoxide: the MOPITT Version 7 product, *Atmos. Meas. Tech.*, 10, 2533-2555, 10.5194/amt-10-2533-2017, 2017.

Ed Dlugokencky, NOAA/GML ([gml.noaa.gov/ccgg/trends\\_ch4/](http://gml.noaa.gov/ccgg/trends_ch4/)), 2022

Emmerson, K. M. and Evans, M. J.: Comparison of tropospheric gas-phase chemistry schemes for use within global models, *Atmos. Chem. Phys.*, 9, 1831-1845, 10.5194/acp-9-1831-2009, 2009.

695 Emmons, L. K., Walters, S., Hess, P. G., Lamarque, J. F., Pfister, G. G., Fillmore, D., Granier, C., Guenther, A., Kinnison, D., Laepple, T., Orlando, J., Tie, X., Tyndall, G., Wiedinmyer, C., Baughcum, S. L., and Kloster, S.: Description and evaluation of the Model for Ozone and Related chemical Tracers, version 4 (MOZART-4), *Geosci. Model Dev.*, 3, 43-67, 10.5194/gmd-3-43-2010, 2010.

Forster, P., T. Storelvmo, K. Armour, W. Collins, J.-L. Dufresne, D. Frame, D.J. Lunt, T. Mauritsen, 700 M.D. Palmer, M. Watanabe, M. Wild, and H. Zhang, 2021: The Earth's Energy Budget, Climate

Feedbacks, and Climate Sensitivity. In *Climate Change 2021: The Physical Science Basis. Contribution of Working Group I to the Sixth Assessment Report of the Intergovernmental Panel on Climate Change* [Masson-Delmotte, V., P. Zhai, A. Pirani, S.L. Connors, C. Pean, S. Berger, N. Caud, Y. Chen, L. Goldfarb, M.I. Gomis, M. Huang, K. Leitzell, E. Lonnoy, J.B.R. Matthews, T.K. Maycock, T. Waterfield, O. Yelekci, R. Yu, and B. Zhou (eds.)]. Cambridge University Press, Cambridge, United Kingdom and New York, NY, USA, pp. 923–1054, 10.1017/9781009157896.009.

Frith, S. M., Kramarova, N. A., Stolarski, R. S., McPeters, R. D., Bhartia, P. K., and Labow, G. J.: Recent changes in total column ozone based on the SBUV Version 8.6 Merged Ozone Data Set, *Journal of Geophysical Research: Atmospheres*, 119, 9735-9751, 10.1002/2014jd021889, 2014.

710 Geddes, J. A. and Martin, R. V.: Global deposition of total reactive nitrogen oxides from 1996 to 2014 constrained with satellite observations of NO<sub>2</sub> columns, *Atmos. Chem. Phys.*, 17, 10071-10091, 10.5194/acp-17-10071-2017, 2017.



- 715 Gelaro, R., McCarty, W., Suárez, M. J., Todling, R., Molod, A., Takacs, L., Randles, C. A., Darmenov, A., Bosilovich, M. G., Reichle, R., Wargan, K., Coy, L., Cullather, R., Draper, C., Akella, S., Buchard, V., Conaty, A., da Silva, A. M., Gu, W., Kim, G.-K., Koster, R., Lucchesi, R., Merkova, D., Nielsen, J. E., Partyka, G., Pawson, S., Putman, W., Rienecker, M., Schubert, S. D., Sienkiewicz, M., and Zhao, B.: The Modern-Era Retrospective Analysis for Research and Applications, Version 2 (MERRA-2), *Journal of Climate*, 30, 5419-5454, 10.1175/jcli-d-16-0758.1, 2017.
- 720 González Abad, G., Liu, X., Chance, K., Wang, H., Kurosu, T. P., and Suleiman, R.: Updated Smithsonian Astrophysical Observatory Ozone Monitoring Instrument (SAO OMI) formaldehyde retrieval, *Atmos. Meas. Tech.*, 8, 19-32, 10.5194/amt-8-19-2015, 2015.
- Hegglin, M. I. and Lamarque, J.-F.: The IGAC/SPARC Chemistry-Climate Model Initiative Phase-1 (CCMI-1) model data output, NCAS British Atmospheric Data Centre, [ADD ACCESS DATE], available at: <http://catalogue.ceda.ac.uk/uuid/> (last access: December 2019), 2015.
- 725 Jackson, R. B., Saunio, S., Bousquet, P., Canadell, J. G., Poulter, B., Stavert, A. R., Bergamaschi, P., Niwa, Y., Segers, A., Tsuruta, A. Increasing anthropogenic methane emissions arise equally from agricultural and fossil fuel sources. *Environmental Research Letters* 15: 071002, 2020.
- Jiang, J. H., Su, H., Zhai, C., Wu, L., Minschwaner, K., Molod, A. M., and Tompkins, A. M.: An assessment of upper troposphere and lower stratosphere water vapor in MERRA, MERRA2, and ECMWF reanalyses using Aura MLS observations, 120, 11,468-411,485, <https://doi.org/10.1002/2015JD023752>, 2015.
- 730 Kirschke, S., Bousquet, P., Ciais, P., Saunio, M., Canadell, J. G., Dlugokencky, E. J., Bergamaschi, P., Bergmann, D., Blake, D. R., Bruhwiler, L., Cameron-Smith, P., Castaldi, S., Chevallier, F., Feng, L., Fraser, A., Heimann, M., Hodson, E. L., Houweling, S., Josse, B., Fraser, P. J., Krummel, P. B., Lamarque, J.-F., Langenfelds, R. L., Le Quéré, C., Naik, V., O'Doherty, S., Palmer, P. I., Pison, I., Plummer, D., Poulter, B., Prinn, R. G., Rigby, M., Ringeval, B., Santini, M., Schmidt, M., Shindell, D. T., Simpson, I. J., Spahni, R., Steele, L. P., Strode, S. A., Sudo, K., Szopa, S., van der Werf, G. R., Voulgarakis, A., van Weele, M., Weiss, R. F., Williams, J. E., and Zeng, G.: Three decades of global methane sources and sinks, *Nature Geoscience*, 6, 813, 10.1038/ngeo1955
- 735 Lamarque, J. F., Emmons, L. K., Hess, P. G., Kinnison, D. E., Tilmes, S., Vitt, F., Heald, C. L., Holland, E. A., Lauritzen, P. H., Neu, J., Orlando, J. J., Rasch, P. J., and Tyndall, G. K.: CAM-chem: description and evaluation of interactive atmospheric chemistry in the Community Earth System Model, *Geosci. Model Dev.*, 5, 369-411, 10.5194/gmd-5-369-2012, 2012.
- 740 Lelieveld, J., Gromov, S., Pozzer, A., and Taraborrelli, D.: Global tropospheric hydroxyl distribution, budget and reactivity, *Atmospheric Chemistry and Physics*, 16, 12477-12493, 10.5194/acp-16-12477-2016, 2016.
- 745 Lelieveld, J., Butler, T. M., Crowley, J. N., Dillon, T. J., Fischer, H., Ganzeveld, L., Harder, H., Lawrence, M. G., Martinez, M., Taraborrelli, D., and Williams, J.: Atmospheric oxidation capacity sustained by a tropical forest, *Nature*, 452, 737-740, 10.1038/nature06870, 2008.



- 750 Levy, H.: Normal Atmosphere: Large Radical and Formaldehyde Concentrations Predicted, *Science*, 173, 141-143, 10.1126/science.173.3992.141, 1971.
- Mar, K. A., Unger, C., Walderdorff, L., and Butler, T.: Beyond CO<sub>2</sub> equivalence: The impacts of methane on climate, ecosystems, and health, *Environmental Science & Policy*, 134, 127-136, <https://doi.org/10.1016/j.envsci.2022.03.027>, 2022.
- 755 Marais, E. A., Roberts, J. F., Ryan, R. G., Eskes, H., Boersma, K. F., Choi, S., Joiner, J., Abuhassan, N., Redondas, A., Grutter, M., Cede, A., Gomez, L., and Navarro-Comas, M.: New observations of NO<sub>2</sub> in the upper troposphere from TROPOMI, *Atmos. Meas. Tech.*, 14, 2389-2408, 10.5194/amt-14-2389-2021, 2021.
- Molod, A., Takacs, L., Suarez, M., Bacmeister, J., Song, I.-S., and Eichmann, A.: The GEOS Atmospheric General Circulation Model: Mean Climate and Development from MERRA to Fortuna, NASA Technical Report Series on Global Modeling and Data Assimilation, NASA TM-2012-104606, 28, 117 pp., 2012.
- 760 Molod, A., Takacs, L., Suarez, M., and Bacmeister, J.: Development of the GEOS-5 atmospheric general circulation model: evolution from MERRA to MERRA2, *Geosci. Model Dev.*, 8, 1339-1356, 10.5194/gmd-8-1339-2015, 2015.
- 765 Monks, S. A., Arnold, S. R., Emmons, L. K., Law, K. S., Turquety, S., Duncan, B. N., Flemming, J., Huijnen, V., Tilmes, S., Langner, J., Mao, J., Long, Y., Thomas, J. L., Steenrod, S. D., Raut, J. C., Wilson, C., Chipperfield, M. P., Diskin, G. S., Weinheimer, A., Schlager, H., and Ancellet, G.: Multi-model study of chemical and physical controls on transport of anthropogenic and biomass burning pollution to the Arctic, *Atmos. Chem. Phys.*, 15, 3575-3603, 10.5194/acp-15-3575-2015, 2015.
- 770 Montzka, S. A., Krol, M., Dlugokencky, E., Hall, B., Jöckel, P., and Lelieveld, J.: Small Interannual Variability of Global Atmospheric Hydroxyl, *Science*, 331, 67-69, 10.1126/science.1197640, 2011.
- Morgenstern, O., Hegglin, M. I., Rozanov, E., amp, apos, Connor, F. M., Abraham, N. L., Akiyoshi, H., Archibald, A. T., Bekki, S., Butchart, N., Chipperfield, M. P., Deushi, M., Dhomse, S. S., Garcia, R. R., 775 Hardiman, S. C., Horowitz, L. W., Jöckel, P., Josse, B., Kinnison, D., Lin, M., Mancini, E., Manyin, M. E., Marchand, M., Marécal, V., Michou, M., Oman, L. D., Pitari, G., Plummer, D. A., Revell, L. E., Saint-Martin, D., Schofield, R., Stenke, A., Stone, K., Sudo, K., Tanaka, T. Y., Tilmes, S., Yamashita, Y., Yoshida, K., and Zeng, G.: Review of the global models used within phase 1 of the Chemistry–Climate Model Initiative (CCMI), *Geoscientific Model Development*, 10, 639-671, 10.5194/gmd-10-639-2017, 780 2017.
- Murray, L. T., Logan, J. A., and Jacob, D. J.: Interannual variability in tropical tropospheric ozone and OH: The role of lightning, *Journal of Geophysical Research: Atmospheres*, 118, 11,468-411,480, 10.1002/jgrd.50857, 2013.
- 785 Naik, V., Voulgarakis, A., Fiore, A. M., Horowitz, L. W., Lamarque, J. F., Lin, M., Prather, M. J., Young, P. J., Bergmann, D., Cameron-Smith, P. J., Cionni, I., Collins, W. J., Dalsøren, S. B., Doherty, R., Eyring, V., Faluvegi, G., Folberth, G. A., Josse, B., Lee, Y. H., MacKenzie, I. A., Nagashima, T., van Noije, T. P.



- 790 C., Plummer, D. A., Righi, M., Rumbold, S. T., Skeie, R., Shindell, D. T., Stevenson, D. S., Strode, S.,  
Sudo, K., Szopa, S., and Zeng, G.: Preindustrial to present-day changes in tropospheric hydroxyl radical  
and methane lifetime from the Atmospheric Chemistry and Climate Model Intercomparison Project  
(ACCMIP), *Atmospheric Chemistry and Physics*, 13, 5277-5298, 10.5194/acp-13-5277-2013, 2013.
- Naus, S., Montzka, S. A., Patra, P. K., and Krol, M. C.: A three-dimensional-model inversion of methyl  
chloroform to constrain the atmospheric oxidative capacity, *Atmos. Chem. Phys.*, 21, 4809-4824,  
10.5194/acp-21-4809-2021, 2021.
- 795 Naus, S., Montzka, S. A., Pandey, S., Basu, S., Dlugokencky, E. J., and Krol, M.: Constraints and biases  
in a tropospheric two-box model of OH, *Atmos. Chem. Phys.*, 19, 407-424, 10.5194/acp-19-407-2019,  
2019.
- Nicely, J. M., Canty, T. P., Manyin, M., Oman, L. D., Salawitch, R. J., Steenrod, S. D., Strahan, S. E.,  
and Strode, S. A.: Changes in Global Tropospheric OH Expected as a Result of Climate Change Over  
the Last Several Decades, *Journal of Geophysical Research: Atmospheres*, 123, 10,774-710,795,  
800 doi:10.1029/2018JD028388, 2018.
- Nisbet, E. G., Manning, M. R., Dlugokencky, E. J., Fisher, R. E., Lowry, D., Michel, S. E., Myhre, C. L.,  
Platt, S. M., Allen, G., Bousquet, P., Brownlow, R., Cain, M., France, J. L., Hermansen, O., Hossaini, R.,  
Jones, A. E., Levin, I., Manning, A. C., Myhre, G., Pyle, J. A., Vaughn, B., Warwick, N. J., and White, J.  
W. C.: Very strong atmospheric methane growth in the four years 2014-2017: Implications for the Paris  
805 Agreement, *Global Biogeochemical Cycles*, 33, 318– 342, doi:10.1029/2018GB006009, 2019.
- Oman, L. D., Douglass, A. R., Ziemke, J. R., Rodriguez, J. M., Waugh, D. W., and Nielsen, J. E.: The  
ozone response to ENSO in Aura satellite measurements and a chemistry-climate simulation, 118, 965-  
976, <https://doi.org/10.1029/2012JD018546>, 2013.
- Oman, L. D., Ziemke, J. R., Douglass, A. R., Waugh, D. W., Lang, C., Rodriguez, J. M., and Nielsen, J.  
810 E.: The response of tropical tropospheric ozone to ENSO, 38, <https://doi.org/10.1029/2011GL047865>,  
2011.
- Patra, P. K., Krol, M. C., Prinn, R. G., Takigawa, M., Mühle, J., Montzka, S. A., Lal, S., Yamashita, Y.,  
Naus, S., Chandra, N., Weiss, R. F., Krummel, P. B., Fraser, P. J., O'Doherty, S., and Elkins, J. W.:  
815 Methyl Chloroform Continues to Constrain the Hydroxyl (OH) Variability in the Troposphere, *Journal  
of Geophysical Research: Atmospheres*, 126, e2020JD033862, <https://doi.org/10.1029/2020JD033862>,  
2021.
- Prather, M. J., Holmes, C. D., and Hsu, J.: Reactive greenhouse gas scenarios: Systematic exploration of  
uncertainties and the role of atmospheric chemistry, *Geophysical Research Letters*, 39, L09803,  
doi:10.1029/2012GL051440, 2012.
- 820 Prinn, R. G., Huang, J., Weiss, R. F., Cunnold, D. M., Fraser, P. J., Simmonds, P. G., McCulloch, A.,  
Harth, C., Salameh, P., O'Doherty, S., Wang, R. H. J., Porter, L., and Miller, B. R.: Evidence for  
Substantial Variations of Atmospheric Hydroxyl Radicals in the Past Two Decades, *Science*, 292, 1882-  
1888, 10.1126/science.1058673, 2001.



- 825 Rigby, M., Montzka, S. A., Prinn, R. G., White, J. W. C., Young, D., O'Doherty, S., Lunt, M. F.,  
Ganesan, A. L., Manning, A. J., Simmonds, P. G., Salameh, P. K., Harth, C. M., Muhle, J., Weiss, R. F.,  
Fraser, P. J., Steele, L. P., Krummel, P. B., McCulloch, A., and Park, S.: Role of atmospheric oxidation  
in recent methane growth, *Proc Natl Acad Sci U S A*, 114, 5373-5377, 10.1073/pnas.1616426114, 2017.
- 830 Sander, S. P., Abbatt, J., Barker, J. R., Burkholder, J. B., Friedl, R. R., Golden, D. M., Huie, R., Kurylo,  
M. J., Moortgat, G. K., Orkin, V. L., and Wine, P. H.: Chemical kinetics and photochemical data for use  
in atmospheric studies evaluation number 17, Pasadena, CA: Jet Propulsion Laboratory, National  
Aeronautics and Space Administration, 2011, 2011.
- 835 Saunois, M., Bousquet, P., Poulter, B., Peregón, A., Ciais, P., Canadell, J. G., Dlugokencky, E. J., Etiope,  
G., Bastviken, D., Houweling, S., Janssens-Maenhout, G., Tubiello, F. N., Castaldi, S., Jackson, R. B.,  
Alexe, M., Arora, V. K., Beerling, D. J., Bergamaschi, P., Blake, D. R., Brailsford, G., Bruhwiler, L.,  
Crevoisier, C., Crill, P., Covey, K., Frankenberg, C., Gedney, N., Höglund-Isaksson, L., Ishizawa, M.,  
Ito, A., Joos, F., Kim, H. S., Kleinen, T., Krummel, P., Lamarque, J. F., Langenfelds, R., Locatelli, R.,  
Machida, T., Maksyutov, S., Melton, J. R., Morino, I., Naik, V., O'Doherty, S., Parmentier, F. J. W.,  
Patra, P. K., Peng, C., Peng, S., Peters, G. P., Pison, I., Prinn, R., Ramonet, M., Riley, W. J., Saito, M.,  
Santini, M., Schroeder, R., Simpson, I. J., Spahni, R., Takizawa, A., Thornton, B. F., Tian, H., Tohjima,  
840 Y., Viovy, N., Voulgarakis, A., Weiss, R., Wilton, D. J., Wiltshire, A., Worthy, D., Wunch, D., Xu, X.,  
Yoshida, Y., Zhang, B., Zhang, Z., and Zhu, Q.: Variability and quasi-decadal changes in the methane  
budget over the period 2000–2012, *Atmos. Chem. Phys.*, 17, 11135-11161, 10.5194/acp-17-11135-2017,  
2017.
- 845 Saunois, M., Bousquet, P., Poulter, B., Peregón, A., Ciais, P., Canadell, J. G., Dlugokencky, E. J., Etiope,  
G., Bastviken, D., Houweling, S., Janssens-Maenhout, G., Tubiello, F. N., Castaldi, S., Jackson, R. B.,  
Alexe, M., Arora, V. K., Beerling, D. J., Bergamaschi, P., Blake, D. R., Brailsford, G., Brovkin, V.,  
Bruhwiler, L., Crevoisier, C., Crill, P., Covey, K., Curry, C., Frankenberg, C., Gedney, N., Höglund-  
Isaksson, L., Ishizawa, M., Ito, A., Joos, F., Kim, H. S., Kleinen, T., Krummel, P., Lamarque, J. F.,  
Langenfelds, R., Locatelli, R., Machida, T., Maksyutov, S., McDonald, K. C., Marshall, J., Melton, J. R.,  
850 Morino, I., Naik, V., O'Doherty, S., Parmentier, F. J. W., Patra, P. K., Peng, C., Peng, S., Peters, G. P.,  
Pison, I., Prigent, C., Prinn, R., Ramonet, M., Riley, W. J., Saito, M., Santini, M., Schroeder, R.,  
Simpson, I. J., Spahni, R., Steele, P., Takizawa, A., Thornton, B. F., Tian, H., Tohjima, Y., Viovy, N.,  
Voulgarakis, A., van Weele, M., van der Werf, G. R., Weiss, R., Wiedinmyer, C., Wilton, D. J., Wiltshire,  
A., Worthy, D., Wunch, D., Xu, X., Yoshida, Y., Zhang, B., Zhang, Z., and Zhu, Q.: The global methane  
855 budget 2000–2012, *Earth Syst. Sci. Data*, 8, 697-751, 10.5194/essd-8-697-2016, 2016.
- 860 Saunois, M., Stavert, A. R., Poulter, B., Bousquet, P., Canadell, J. G., Jackson, R. B., Raymond, P. A.,  
Dlugokencky, E. J., Houweling, S., Patra, P. K., Ciais, P., Arora, V. K., Bastviken, D., Bergamaschi, P.,  
Blake, D. R., Brailsford, G., Bruhwiler, L., Carlson, K. M., Carrol, M., Castaldi, S., Chandra, N.,  
Crevoisier, C., Crill, P. M., Covey, K., Curry, C. L., Etiope, G., Frankenberg, C., Gedney, N., Hegglin,  
M. I., Höglund-Isaksson, L., Hugelius, G., Ishizawa, M., Ito, A., Janssens-Maenhout, G., Jensen, K. M.,



- 865 Joos, F., Kleinen, T., Krummel, P. B., Langenfelds, R. L., Laruelle, G. G., Liu, L., Machida, T., Maksyutov, S., McDonald, K. C., McNorton, J., Miller, P. A., Melton, J. R., Morino, I., Müller, J., Murguia-Flores, F., Naik, V., Niwa, Y., Noce, S., O'Doherty, S., Parker, R. J., Peng, C., Peng, S., Peters, G. P., Prigent, C., Prinn, R., Ramonet, M., Regnier, P., Riley, W. J., Rosentreter, J. A., Segers, A., Simpson, I. J., Shi, H., Smith, S. J., Steele, L. P., Thornton, B. F., Tian, H., Tohjima, Y., Tubiello, F. N., Tsuruta, A., Viovy, N., Voulgarakis, A., Weber, T. S., van Weele, M., van der Werf, G. R., Weiss, R. F., Worthy, D., Wunch, D., Yin, Y., Yoshida, Y., Zhang, W., Zhang, Z., Zhao, Y., Zheng, B., Zhu, Q., Zhu, Q., and Zhuang, Q.: The Global Methane Budget 2000–2017, *Earth Syst. Sci. Data*, 12, 1561–1623, 10.5194/essd-12-1561-2020, 2020.
- 870 Spivakovsky, C. M., Logan, J. A., Montzka, S. A., Balkanski, Y. J., Foreman-Fowler, M., Jones, D. B. A., Horowitz, L. W., Fusco, A. C., Brenninkmeijer, C. A. M., Prather, M. J., Wofsy, S. C., and McElroy, M. B.: Three-dimensional climatological distribution of tropospheric OH: Update and evaluation, *Journal of Geophysical Research: Atmospheres*, 105, 8931–8980, 10.1029/1999jd901006, 2000.
- 875 Strode, S. A., Duncan, B. N., Yegorova, E. A., Kouatchou, J., Ziemke, J. R., and Douglass, A. R.: Implications of carbon monoxide bias for methane lifetime and atmospheric composition in chemistry climate models, *Atmos. Chem. Phys.*, 15, 11789–11805, 10.5194/acp-15-11789-2015, 2015.
- Tilmes, S., Lamarque, J. F., Emmons, L. K., Kinnison, D. E., Marsh, D., Garcia, R. R., Smith, A. K., Neely, R. R., Conley, A., Vitt, F., Val Martin, M., Tanimoto, H., Simpson, I., Blake, D. R., and Blake, N.: Representation of the Community Earth System Model (CESM1) CAM4-chem within the Chemistry-Climate Model Initiative (CCMI), *Geosci. Model Dev.*, 9, 1853–1890, 10.5194/gmd-9-1853-2016, 2016.
- 880 Tilmes, S., Lamarque, J. F., Emmons, L. K., Kinnison, D. E., Ma, P. L., Liu, X., Ghan, S., Bardeen, C., Arnold, S., Deeter, M., Vitt, F., Ryerson, T., Elkins, J. W., Moore, F., Spackman, J. R., and Val Martin, M.: Description and evaluation of tropospheric chemistry and aerosols in the Community Earth System Model (CESM1.2), *Geosci. Model Dev.*, 8, 1395–1426, 10.5194/gmd-8-1395-2015, 2015.
- 885 Turner, A. J., Frankenberg, C., Wennberg, P. O., and Jacob, D. J.: Ambiguity in the causes for decadal trends in atmospheric methane and hydroxyl, *Proc Natl Acad Sci U S A*, 114, 5367–5372, 10.1073/pnas.1616020114, 2017.
- Turner, A. J., Fung, I., Naik, V., Horowitz, L. W., and Cohen, R. C.: Modulation of hydroxyl variability by ENSO in the absence of external forcing, *Proceedings of the National Academy of Sciences*, 115, 8931–8936, 10.1073/pnas.1807532115, 2018.
- 890 Zhang, Y., Cooper, O. R., Gaudel, A., Thompson, A. M., Nédélec, P., Ogino, S.-Y., and West, J. J.: Tropospheric ozone change from 1980 to 2010 dominated by equatorward redistribution of emissions, *Nature Geoscience*, 9, 875–879, 10.1038/ngeo2827, 2016.
- Zhao, Y., Saunio, M., Bousquet, P., Lin, X., Berchet, A., Hegglin, M. I., Canadell, J. G., Jackson, R. B., Deushi, M., Jöckel, P., Kinnison, D., Kirner, O., Strode, S., Tilmes, S., Dlugokencky, E. J., and Zheng, B.: On the role of trend and variability in the hydroxyl radical (OH) in the global methane budget, *Atmos. Chem. Phys.*, 20, 13011–13022, 10.5194/acp-20-13011-2020, 2020.



- 900 Zhao, Y., Saunio, M., Bousquet, P., Lin, X., Berchet, A., Hegglin, M. I., Canadell, J. G., Jackson, R. B.,  
Hauglustaine, D. A., Szopa, S., Stavert, A. R., Abraham, N. L., Archibald, A. T., Bekki, S., Deushi, M.,  
Jöckel, P., Josse, B., Kinnison, D., Kirner, O., Marécal, V., O'Connor, F. M., Plummer, D. A., Revell, L.  
E., Rozanov, E., Stenke, A., Strode, S., Tilmes, S., Dlugokencky, E. J., and Zheng, B.: Inter-model  
comparison of global hydroxyl radical (OH) distributions and their impact on atmospheric methane over  
the 2000–2016 period, *Atmos. Chem. Phys.*, 19, 13701-13723, 10.5194/acp-19-13701-2019, 2019.
- 905 Zheng, B., Chevallier, F., Yin, Y., Ciais, P., Fortems-Cheiney, A., Deeter, M. N., Parker, R. J., Wang, Y.,  
Worden, H. M., and Zhao, Y.: Global atmospheric carbon monoxide budget 2000–2017 inferred from  
multi-species atmospheric inversions, *Earth Syst. Sci. Data*, 11, 1411-1436, 10.5194/essd-11-1411-2019,  
2019.
- 910 Ziemke, J. R., Chandra, S., Duncan, B. N., Froidevaux, L., Bhartia, P. K., Levelt, P. F., and Waters, J. W.:  
Tropospheric ozone determined from Aura OMI and MLS: Evaluation of measurements and comparison  
with the Global Modeling Initiative's Chemical Transport Model, 111,  
915 <https://doi.org/10.1029/2006JD007089>, 2006.
- 920
- 925
- 930



935

**Table 1.** The DSMACC model experiments.

Species	Simulations	Description
Ref	Ref_model	Chemical species and meteorological conditions from 3D model simulations for 2010.
All	All_obs	All the chemical species and meteorological conditions listed below adjusted to match observations.
NO <sub>2</sub>	NO2_obs_PBL	Adjust boundary layer NO <sub>2</sub> to match the OMI QA4ECV product.
O <sub>3</sub>	O3_obs	Adjust tropospheric O <sub>3</sub> to match OMI/MLS product.
CH <sub>4</sub>	CH4_obs	Adjust tropospheric CH <sub>4</sub> to match the assimilated data.
CO	CO_obs	Adjust tropospheric CO to match the assimilated data.
CH <sub>2</sub> O	CH2O_obs	Adjust tropospheric CH <sub>2</sub> O to match the assimilated data.
O <sub>3</sub> column	O3col_obs	Adjust total ozone column to match SBUV/MOD data.
H <sub>2</sub> O <sub>(g)</sub>	H2O_obs	Adjust water vapor to MERRA-2 data.
Ta	Ta_obs	Adjust air temperatures to MERRA-2 data.

**Table 2.** Modeled and observation-based estimates of global [OH]<sub>trop-M</sub>, CH<sub>4</sub> sink by tropospheric OH (L<sub>CH<sub>4</sub>+OH</sub>) averaged during 2000-2009, and the CH<sub>4</sub> lifetime against tropospheric OH.

		[OH] <sub>trop-M</sub> (10 <sup>5</sup> molec cm <sup>-3</sup> )	L <sub>CH<sub>4</sub>+OH</sub> (Tg yr <sup>-1</sup> )	CH <sub>4</sub> lifetime(yr)
Modeled	CESM1-CAM4chem	11.9	540	9.1
	GEOSCCM	12.6	565	8.7
Observation-based	CESM1-CAM4chem	9.9	434	11.4
	GEOSCCM	10.4	461	10.7

940

**Table 3.** The modeled and observation-based [OH]<sub>trop-M</sub> (in 10<sup>5</sup>molec cm<sup>-3</sup>) averaged over latitudinal bands during 2000-2009. The corresponding tropospheric CH<sub>4</sub> sink by OH (L<sub>CH<sub>4</sub>+OH</sub>) (in Tg yr<sup>-1</sup>) is given in brackets.

		90°-30°S	30°S-0°	0°-30°N	30°-90°N
Modeled	CESM1-CAM4chem	5.9(49)	14.2(173)	17.8(226)	9.4(93)
	GEOSCCM	6.2(50)	16.1(192)	18.5(229)	9.6(94)
Observation-based	CESM1-CAM4chem	5.3(42)	12.2(144)	14.5(178)	7.2(69)
	GEOSCCM	5.6(46)	13.6(161)	14.9(183)	7.4(72)

945



**Table 4.** Contributions from individual factors to the difference in global  $[\text{OH}]_{\text{trop-M}}$  and tropospheric  $\text{CH}_4$  sink by reaction with OH between CESM1-CAM4chem simulated and the corresponding observation-based OH fields (modeled – observation-based).

	$[\text{OH}]_{\text{trop-M}}$ ( $10^5 \text{ molec cm}^{-3}$ )	$\text{CH}_4$ sink ( $\text{Tg yr}^{-1}$ )
$\text{H}_2\text{O}_{(\text{g})}$	0.1	10
$\text{T}_a$	0	0
Column $\text{O}_3$	0.4	22
CO	1.3	60
$\text{O}_3$	-0.3	-17
$\text{NO}_2$	0.3	22
$\text{CH}_4$	0.1	5
$\text{CH}_2\text{O}$	0.1	6
<b>Total</b>	2.0	108

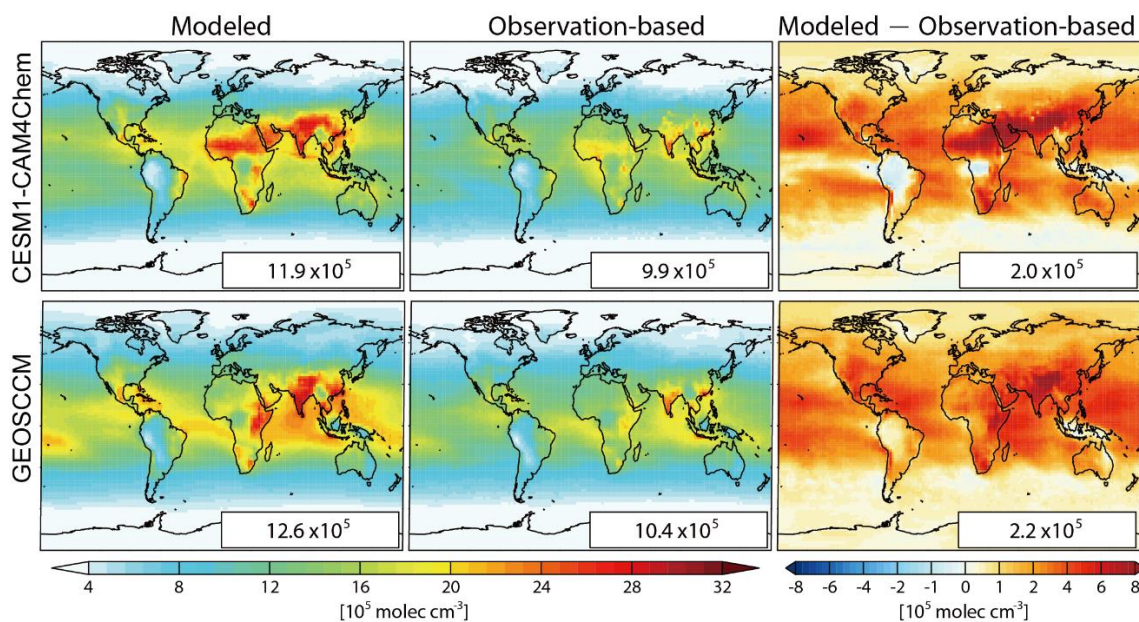


**Figure 1.** Spatial distributions of air mass-weighted tropospheric mean  $[\text{OH}]$  ( $[\text{OH}]_{\text{trop-M}}$ ) in 2010 from model simulations (left) and constrained by observations (middle), and the difference between modeled and observation-based  $[\text{OH}]_{\text{trop-M}}$  (right) estimated from CESM1-CAM4Chem (top) and GEOSCCM (bottom) simulations. The global mean values are shown inset in  $\text{molec cm}^{-3}$ .

955

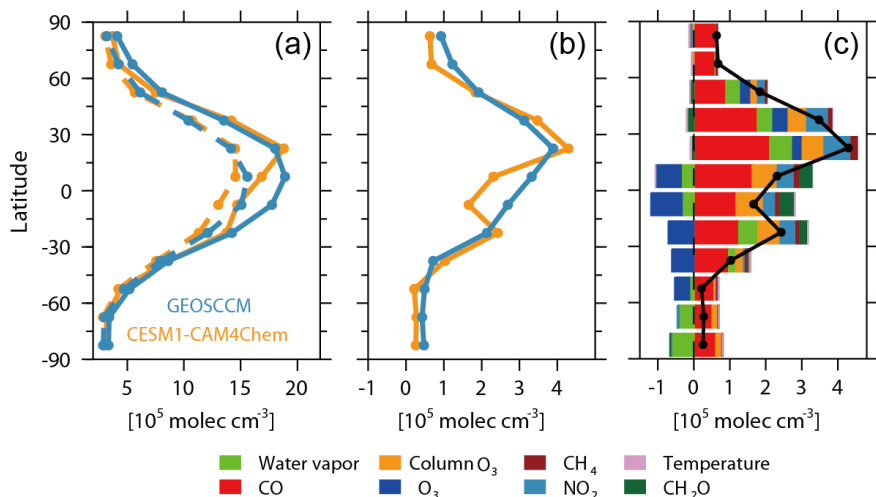


**Figure 2.** (a) Zonal averaged  $[\text{OH}]_{\text{trop-M}}$  of modeled (solid lines) and observation-based OH field (dashed lines) estimated from CESM1 CAM4-chem (yellow) and GEOSCCM (blue) simulations. (b) Difference of zonal averaged  $[\text{OH}]_{\text{trop-M}}$  between modeled and observation-based OH fields. (c) Difference between CESM1 CAM4-chem simulated and observational-based zonal averaged  $[\text{OH}]_{\text{trop-M}}$  (black line) and the contribution from each OH precursor (colored bars) for zonal averaged difference.

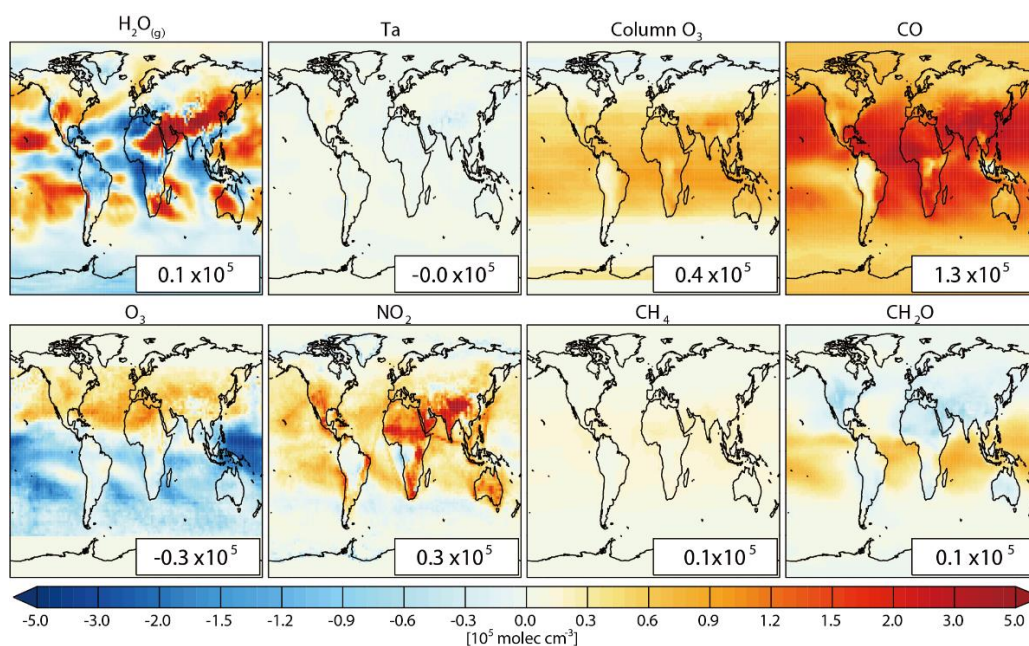
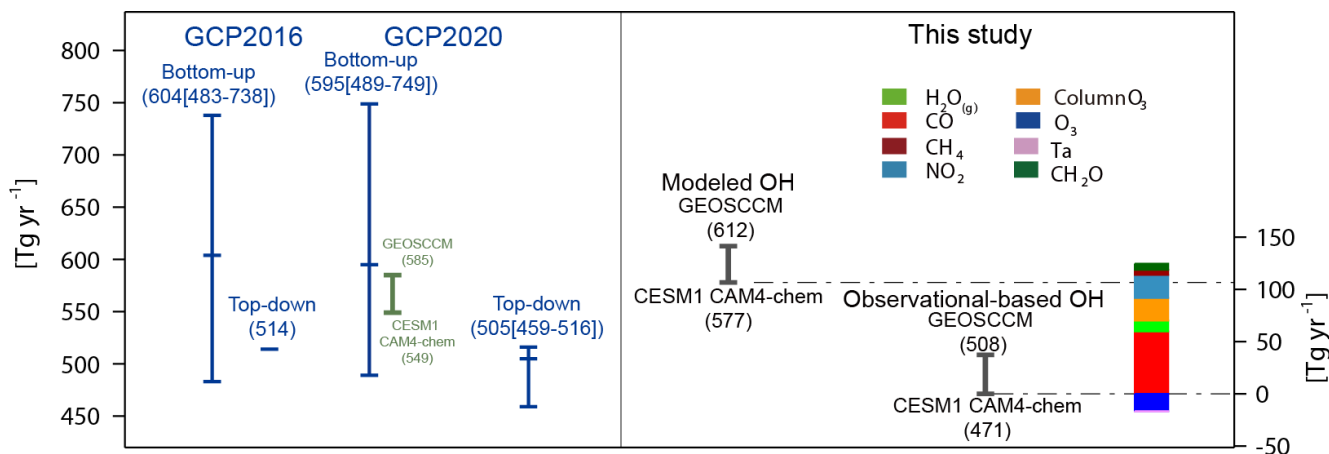


**Figure 3.** Spatial distributions of the contribution of individual factors to the difference between CESM1 CAM4-chem simulated and observation-based (modeled – observation-based)  $[\text{OH}]_{\text{trop-M}}$ . The global mean values are shown inset in  $\text{molec cm}^{-3}$ .



970

**Figure 4.** Global total chemical loss of CH<sub>4</sub> estimated by the bottom-up and top-down methods from previous GCP global CH<sub>4</sub> budget (blue bars; Saunois et al., 2016; 2020), simulated by GEOSCCM and CESM1 CAM4-Chem which is included in the bottom-up estimates in Saunois et al. (2020) (green bar), and that estimated in this study using the model simulated and observation-based OH fields and assimilated surface observations of CH<sub>4</sub> (black bars). The colored bar shows the contribution of individual factors to the difference in the chemical loss of CH<sub>4</sub> between CESM1 CAM4-Chem simulated and the corresponding observation-based OH. The blue, green, and black bars are corresponding to the left axis and the colored bar is corresponding to the right axis.

975

980

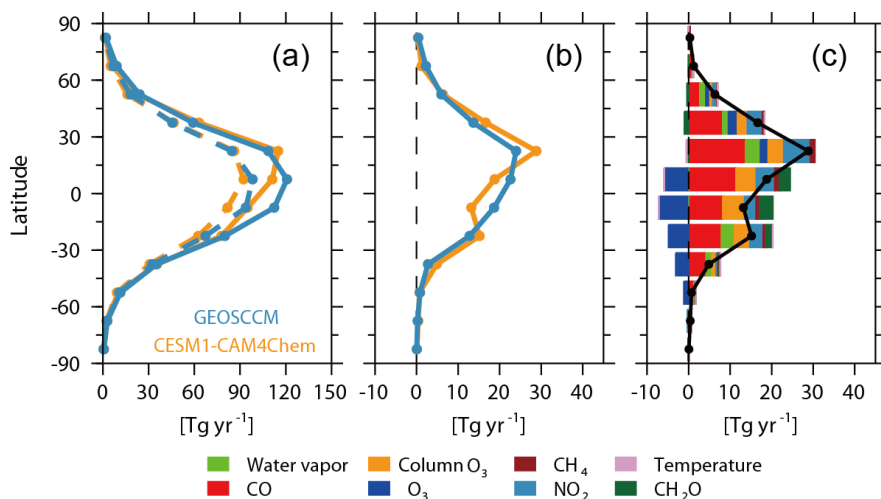


**Figure 5.** Same as Fig.2 but for the tropospheric CH<sub>4</sub> sink by reaction with OH.